

1 **Loss of Zfp335 triggers cGAS/STING-dependent apoptosis of post- $\beta$  selection**  
2 **pre-T cells**

3 Jeremy J Ratiu<sup>1\*</sup>, Qun Wang<sup>1</sup>, Naren Mehta<sup>1</sup>, Melissa J Harnois<sup>1</sup>, Devon DiPalma<sup>1</sup>,  
4 Sebastian Wellford<sup>1</sup>, Sumedha Roy<sup>1</sup>, Alejandra V Contreras<sup>2</sup>, David Wiest<sup>2</sup>, Yuan  
5 Zhuang<sup>1</sup>

6 <sup>1</sup> Duke University, Department of Immunology, Durham, NC 27710

7 <sup>2</sup> Fox Chase Cancer Center, Blood Cell Development and Function Program,  
8 Philadelphia, PA 19111

9 \* Correspondence: [Jeremy.Ratiu@duke.edu](mailto:Jeremy.Ratiu@duke.edu)

10

11 **Abstract**

12 Production of a diverse peripheral T cell compartment requires massive  
13 expansion of the bone marrow progenitors that seed the thymus. There are two main  
14 phases of expansion during T cell development, following T lineage commitment at the  
15 DN2 stage and following successful rearrangement and selection for functional TCR $\beta$   
16 chains in DN3 thymocytes, which promotes development of DN4 cells to the DP stage.  
17 Signals driving expansion of DN2 thymocytes are well studied, however, factors  
18 regulating the proliferation and survival of DN4 cells remain poorly understood. Here,  
19 we uncover an unexpected link between the transcription factor Zfp335 and control of  
20 cGAS/STING-dependent cell death in post- $\beta$ -selection DN4 thymocytes. Zfp335 controls  
21 survival by sustaining expression of Ankle2, which suppresses cGAS/STING-dependent  
22 cell death. Together, this study identifies Zfp335 as a key transcription factor controlling

23 the survival of proliferating post- $\beta$ -selection thymocytes and demonstrates a key role for  
24 the cGAS/STING pathway driving apoptosis of developing T cells.

## 25 **Introduction**

26 Development of large number of T cells with clonally acquired T cell receptor  
27 (TCR) in the thymus demands a small number of bone marrow derived progenitors to  
28 undergo vigorous expansion prior to each of the sequentially ordered TCR gene  
29 rearrangement events. The first major expansion occurs immediately upon T lineage  
30 commitment at the DN2 stage prior to rearrangement of any TCR gene<sup>1, 2, 3, 4</sup>. The  
31 expanded T cell progenitors enter the DN3 stage where rearrangement at the TCR $\beta$ ,  $\gamma$ ,  
32  $\delta$  gene loci become permissive. In postnatal thymus, the majority of DN3 cells will  
33 choose the  $\alpha\beta$ T cell fate due to the generation of a productively rearranged TCR $\beta$  chain.  
34 Post  $\beta$ -selection DN3 cells then move to the DN4 stage where the second phase of  
35 expansion occurs, typically involving several rounds of rapid proliferation over the  
36 course of 2-3 days in mice. The expansion of TCR $\beta$  positive cells result in generation of  
37 the post mitotic DP cells, which constitutes 90% of all thymocytes in post-natal mice and  
38 humans. DP cells undergo TCR $\alpha$  gene rearrangement and selection, a process  
39 resulting in approximately 1% of cells surviving and contributing to the peripheral T cell  
40 pool. Therefore, the expansion of post  $\beta$ -selection DN4 cells prior to TCR $\alpha$  gene  
41 rearrangement and TCR selection represents a critical amplifier to control the output of  
42  $\alpha\beta$ T cells from the thymus.

43 While most stages of T cell development have been subject to extensive genetic  
44 and functional characterization, the post- $\beta$ -selection proliferative phase remains less

45 well understood. Previous studies have shown that proliferation but not survival of DN4  
46 cells is dependent upon IL-7R signaling which functions to repress Bcl6 expression<sup>5</sup>.  
47 Similarly, proliferation during this stage of development also requires the combined  
48 activities of NOTCH and pre-TCR signaling<sup>6, 7, 8, 9</sup>. This effect is in part the result of  
49 induction of Fbxl1 and Fbxl12 which induce polyubiquitination and proteasomal  
50 degradation of Cdkn1b ensuring proper cell cycle progression and proliferation<sup>10</sup>.  
51 Survival of proliferating post- $\beta$ -selection thymocytes was found to require expression of  
52 the chromatin associated protein yin yang 1 (Yy1), the absence of which drives p53-  
53 dependent apoptosis<sup>11</sup>. Animal models exploring cell death during T cell development  
54 have repeatedly shown thymocyte apoptosis, including among DN4 cells, is largely  
55 driven by activities of pro-apoptotic Bcl2 family proteins<sup>12, 13, 14, 15, 16</sup>. Pathways  
56 controlling the survival and death of early proliferating thymocytes upstream of the Bcl2  
57 family remain largely unexplored.

58 Underpinning the fate decisions of thymocytes are vast transcriptional networks  
59 which coordinate the intricate changes and checkpoint traversals required for proper  
60 development<sup>17</sup>. Numerous transcription factors function at different stages to achieve  
61 this result. One transcription factors family of particular importance are the basic helix-  
62 loop-helix E proteins, which include E2A, HEB and E2-2. In developing T cells, activities  
63 of the E2A and HEB have been shown to regulate nearly all stages of thymopoiesis<sup>18</sup>,  
64<sup>19</sup>. These E proteins play critical roles in enforcing the  $\beta$ -selection checkpoint by  
65 promoting expression of *Rag1/2*<sup>20</sup> and *pre-T $\alpha$* <sup>21</sup>, activation of the TCR $\beta$ <sup>22</sup>, TCR $\gamma$ , and  
66 TCR $\delta$  loci<sup>23</sup> and preventing passage of DN cells lacking a functional TCR $\beta$  chain from  
67 progressing to the DP stage<sup>24, 25</sup>. Additionally, E protein activity has been shown to

68 enforce early T cell lineage commitment <sup>26</sup> and promote survival of post- $\beta$ -selection DP  
69 thymocytes undergoing TCR $\alpha$  recombination <sup>27</sup>. Together, the combined activities of E  
70 proteins play critical and indispensable roles in the establishment of a functional T cell  
71 repertoire. However, due to the widespread binding of these factors throughout the  
72 genome of developing thymocytes our understanding of their roles in development are  
73 far from complete.

74 The cGAS/STING pathway functions to sense cytosolic DNA and initiate innate  
75 immune responses <sup>28</sup>. Cyclic GMP-AMP (cGAMP) synthase (cGAS) recognizes dsDNA,  
76 typically of foreign origin, catalyzing the generation of the cyclic dinucleotide (CDN)  
77 second messenger cGAMP which in turn drives STING activation and down-stream  
78 signaling <sup>29</sup>. The cGAS/STING pathway is best known for its functions in non-immune  
79 and innate immune cells such as macrophage and dendritic cells in the context of viral  
80 or bacterial infections. In these contexts, activation of the pathway typically results in the  
81 production of type I interferons and other pro-inflammatory mediators. Recent work has  
82 shown that the cGAS/STING pathway is also highly active but functionally divergent  
83 within T cells, primarily driving type I interferon-independent responses and apoptosis <sup>30</sup>,  
84 <sup>31, 32, 33</sup>. Under steady-state conditions the cGAS/STING pathway plays a minimal role in  
85 T cell development as evidenced by normal thymic T cell subset proportions and overall  
86 thymus size in cGAS or STING-deficient C57/BL6 mice <sup>32</sup>. However, it remains to be  
87 determined whether the cGAS/STING pathway plays a role in sensing and responding  
88 to cell intrinsic stresses during thymic T cell development.

89 In this study we show that loss of Zinc finger transcription factor 335 (Zfp335),  
90 triggered cGAS/STING-mediated apoptosis among proliferating DN4 cells. Zfp335 was

91 initially identified from genetic mapping of familial traits that cause a severe form of  
92 microcephaly<sup>34</sup>. Using a conditional knockout mouse model<sup>34, 35</sup> we show that loss of  
93 Zfp335 promotes cGAS/STING dependent apoptosis among proliferating post- $\beta$ -  
94 selection DN4 thymocytes, severe reduction in overall thymic cellularity and a near  
95 absence of peripheral T cells. Mechanistically, Zfp335 functions to suppress  
96 cGAS/STING activation through promoting Ankle2 expression which in turn regulates  
97 the cGAS inhibitor Baf<sup>36</sup>. The importance of cGAS/STING pathway among DN4  
98 thymocytes was further demonstrated by their sensitivity to STING agonist and STING-  
99 mediated cell death in wild type mice. Thus, we have uncovered for the first time a role  
100 for the cGAS/STING pathway in regulating thymic T cell development and identify the  
101 Zfp335/Ankle2/Baf axis as the first transcriptional network functioning to regulate  
102 cGAS/STING activity.

103

## 104 **Results**

### 105 Zfp335, an E-protein target, is critical for T cell development

106 The E protein family of transcription factors are indispensable regulators of nearly  
107 every stage of T cell development<sup>4, 17, 22, 24, 27, 37, 38, 39, 40</sup>. E proteins control complex  
108 transcriptional networks which remain incompletely understood. To gain deeper insight  
109 into mechanisms by which E proteins regulate T cell development, we previously  
110 performed E2A ChIP-seq to identify the genome-wide binding sites during T cell  
111 development<sup>40</sup>. We identified Zfp335 as an E protein target during T cell development  
112 (Supp Fig 1A). Analysis of published data showed E protein-deficient thymocytes exhibit

113 significantly reduced *Zfp335* expression (Supp Fig 1B)<sup>39</sup>. Since germline deletion of  
114 *Zfp335* is non-viable<sup>34</sup> we utilized a conditional deletion model driven in which Cre  
115 expression is controlled by the E8<sub>III</sub> enhancer of *Cd8a* (E8<sub>III</sub>-cre) to allow functional  
116 assessment of *Zfp335* in post- $\beta$ -selection thymocytes<sup>35</sup>. There are conflicting reports  
117 regarding the deletion kinetics for this Cre<sup>35, 41</sup>, therefore, we began by assessing its  
118 activity across T cell development in our system (Supp Fig 1C-D). Consistent with  
119 Dashtsoodol *et al.*, we found E8<sub>III</sub>-cre is highly active immediately upon entry into DN3a  
120 with no recombination activity evident in the preceding DN2 stage. However,  
121 recombination does not appear to be complete until the DP stage.

122 We subsequently assessed *Zfp335<sup>fl/fl</sup>* E8<sub>III</sub>-cre (*Zfp335cKO*) mice for thymic T cell  
123 development. Deletion of *Zfp335* led to a significant reduction in total thymic cellularity  
124 (Fig 1A-B). This reduction in thymic cellularity is likely due to defects in the  $\alpha\beta$  lineage  
125 as numbers of  $\gamma\delta$  T cells were not altered (Fig 1C-D). Assessment of developmental  
126 stages revealed the reduction in thymocyte numbers of *Zfp335cKO* mice begins at the  
127 DN4 stage (Fig 1E-I).

128 Examination of the peripheral T cell compartment revealed significantly reduced  
129 numbers of splenic T cells in *Zfp335cKO* mice (Supp Fig 2A-K). A previous study  
130 identified the hypomorphic *Zfp335<sup>bloto</sup>* allele as the causative mutation in a unique form  
131 of T lymphopenia<sup>42</sup>. Like *Zfp335<sup>bloto</sup>* mice, we found that peripheral T cells in *Zfp335cKO*  
132 mice were almost exclusively of an effector or memory phenotype suggesting these  
133 mice also exhibit a similar defect in the establishment of the naïve T cell compartment.

134 To determine the transcriptional changes resulting from loss of *Zfp335* we  
135 performed RNA-seq on *Zfp335cKO* DP thymocytes. DP cells were used as they were

136 the first population exhibiting complete deletion (Supp Fig 1D). We found that loss of  
137 *Zfp335* results in differential expression of 327 genes (113 down, 214 up; Fig 1K,J).  
138 Among the 161 *Zfp335* ChIP-seq targets identified in thymocytes<sup>42</sup>, 34 were down-  
139 regulated in *Zfp335*cKO mice (Fig 1K). No *Zfp335* target genes were up-regulated in  
140 *Zfp335*cKO samples (Fig 1K) corroborating previous findings that *Zfp335* primarily  
141 functions as a transcriptional activator<sup>34, 42</sup>. Consistent with transcriptomic analyses of  
142 *Zfp335*<sup>*bloto*</sup> mice<sup>42</sup>, gene set enrichment analysis (GSEA) revealed significant enrichment  
143 among type I and type III interferon signaling and P53 signaling pathways in *Zfp335*cKO  
144 DP cells (Fig 1L). Together, these findings identify *Zfp335* as a key transcription factor  
145 regulating T cell development.

#### 146 Loss of *Zfp335* in DN3 thymocytes does not impair $\beta$ -selection

147 *Zfp335* deletion results in reduced cell numbers beginning at the DN4 stage,  
148 raising the possibility that the inability to rearrange the TCR $\beta$  locus could be  
149 responsible. Consequently, we assessed TCR $\beta$  rearrangement in DN3 and DN4  
150 thymocytes by intracellular staining. The frequency of icTCR $\beta$ <sup>+</sup> cells among *Zfp335*cKO  
151 DN3 and DN4 subsets was comparable to that of WT (Supp Fig 3A-C). Therefore,  
152 TCR $\beta$  rearrangement and subsequent pre-TCR expression are unimpaired in  
153 *Zfp335*cKO mice.

154 In addition to pre-TCR expression, to successfully traverse the  $\beta$ -selection  
155 checkpoint, pre-TCR signals are required for release from cell cycle arrest, survival and  
156 progression to DP<sup>43</sup>. CD27 surface expression is increased by pre-TCR signals in DN3  
157 thymocytes<sup>44</sup>. *Zfp335*cKO DN3 thymocytes exhibited CD27 upregulation comparable to  
158 that of WT (Supp Fig 3D-E) indicating *Zfp335*-deficiency does not lead to impaired pre-

159 TCR signaling. Together, these results indicate that the observed reduction of DN4 cells  
160 in Zfp335cKO mice did not result from failure to produce TCR $\beta$  subunits or failure to  
161 transduce pre-TCR signals.

162

### 163 Zfp335 inhibits apoptosis during the DN-DP transition

164 Zfp335 deletion during the DN3 stage leads to severe defects in T cell  
165 development, likely during the post- $\beta$ -selection proliferative phase. To determine if  
166 Zfp335-deficiency altered either the proliferation or survival of post- $\beta$  selection  
167 thymocytes, we directly measured these events in OP9-DL1 cultures *in vitro*<sup>45</sup>. DN3a  
168 thymocytes were cultured on OP9-DL1 cells then assessed for developmental  
169 progression. Consistent with our *ex vivo* data, Zfp335cKO cells exhibit severely  
170 impaired progression to the DP stage (Fig 2A-B). Zfp335cKO cells exhibited modestly  
171 reduced proliferation compared to controls (Fig 2C-D). In contrast, Zfp335cKO cells  
172 underwent substantially increased rates of apoptosis (Fig 2E-F). Importantly,  
173 proliferation tracking (Fig 2G) and assessment of developmental progression (Fig 2H) of  
174 apoptotic mutant cells demonstrate they have undergone cell division and Zfp335-  
175 deficient apoptotic cells largely remain DN. These data suggest that Zfp335cKO cells  
176 are dying during the post- $\beta$ -selection proliferative phase and that Zfp335 activity  
177 promotes the survival of DN4 thymocytes.

178

### 179 Ectopic Bcl2 expression rescues the developmental defect resulting from loss of Zfp335



180 Our RNA-seq studies revealed Zfp335cKO thymocytes exhibit increased  
181 expression of the pro-apoptotic Bcl2-family members, PUMA (*Bbc3*), NOXA (*Pmaip1*)  
182 and *Bax* (Fig 3A), suggesting that these factors may be responsible for the observed  
183 increase in apoptosis among Zfp335cKO thymocytes. The function of these proteins  
184 can be antagonized by ectopic expression Bcl2. Thus, we asked whether Bcl2  
185 overexpression could rescue Zfp335cKO thymocyte apoptosis. WT or Zfp335cKO  
186 DN3/4 thymocytes were transduced with control or Bcl2-expressing retroviruses then  
187 grown in the OP9-DL1 culture system. Bcl2 overexpression significantly reduced  
188 apoptosis in Zfp335cKO cells, indicating the induction of pro-apoptotic Bcl2 family  
189 members was at least partially responsible for the observed increase in apoptosis in  
190 Zfp335-deficient thymocytes (Fig 3B-C).

191 We next sought to test the ability of Bcl2 overexpression to rescue Zfp335-  
192 deficient cells from apoptosis *in vivo* through generating Bcl2 conditional transgenic  
193 mice (Fig 3D). Intracellular staining revealed that *Zfp335<sup>fl/fl</sup> R26<sup>LSL-Bcl2-Tg</sup> E8III-cre*  
194 (Zfp335cKO Bcl2-Tg) thymocytes exhibited increased Bcl2 protein expression relative to  
195 WT (Fig 4E). Phenotypic analysis demonstrated that ectopic Bcl2 expression was able  
196 to fully rescue the early developmental defects observed in Zfp335-deficient mice,  
197 restoring traversal of the  $\beta$ -selection checkpoint, transition to the DP stage, and total  
198 thymic cellularity (Fig 3F-L).

199 Consistent with studies of *Zfp335<sup>bloto</sup>* mice<sup>42</sup>, Bcl2 overexpression failed to rescue  
200 the impairment in final single positive thymocyte maturation (Supp Fig 4A-C) or  
201 peripheral T cell compartment numbers (Supp Fig 4D-E) and effector status (Supp Fig  
202 4F-H). Taken together, these data suggest that the early impairment of thymocyte

203 development following loss of Zfp335 expression is due to increased rates of DN4  
204 apoptosis driven by pro-apoptotic Bcl2-family members. However, our *in vivo* studies  
205 also revealed an additional, Bcl2-independent late block in terminal T cell differentiation  
206 within the thymus.

207

### 208 Defining the 'true' DN4 thymocyte population at the single cell level

209 The DN4 stage of T cell development remains poorly understood and, as a  
210 result, poorly defined. DN4 cells are identified by lack of expression of identifying  
211 markers associated with any other thymocyte subset. Based on these criteria, it is  
212 possible that DN4 cells defined by marker exclusion may not be homogenous. To  
213 assess whether there is any heterogeneity in the DN4 compartment exacerbated by  
214 Zfp335-deficiency, we performed scRNA-seq of phenotypically defined DN4 cells. After  
215 quality control, libraries yielded transcriptome data for 6,537 or 5,392 high-quality cells  
216 from WT or Zfp335cKO samples, respectively.

217 We identified 10 unique cell clusters (Fig 4A-C). Five clusters were largely  
218 cycling cells (DN4\_1-5; Fig 4A-B) uniquely expressing *Ptcra* (pre-T $\alpha$ ) and proliferation  
219 associated genes (*Mki67*, *Cdk1*) (Fig 4D), representing bona fide DN4 cells. Three  
220 clusters (Mat\_1-3) expressed high levels of *Trac* and *Trbc1* transcripts (Fig 4D). Two  
221 additional clusters (gd17 and gd1) of  $\gamma\delta$  T cells were identified. gd17 cells express high  
222 levels of *Sox13*, *Rorc* and *Maf*, features of  $\gamma\delta$ 17 while gd1 express *Nkg7*, *Ii2rb*, *S1pr1*  
223 and *Ii7r* associated with cytotoxic  $\gamma\delta$  T cells (Fig 4D). Based on this clustering, Zfp335-

224 deficiency led to substantial proportional increases and decreases in the  $\gamma\delta$  T cell  
225 clusters and Mat\_2 cluster relative to WT control, respectively (Fig 4C).

226 We were surprised to find a large proportion of phenotypically defined DN4  
227 thymocytes expressing *Trac* transcripts and sought to define these populations.  
228 Consistent with their lack of surface CD4 or CD8 these cells uniformly lacked *Cd4*,  
229 *Cd8a* and *Cd8b1* transcripts (Fig 4D). We hypothesized that these cells may represent  
230 post-positive selection thymocytes that transiently down-regulated surface TCR, CD4  
231 and CD8 expression. Consistent with our hypothesis, we found these cells express high  
232 levels of *Nr4a1*, *Cd69*, *Pdcd1*, *Egr1*, *Cd2*, and *Itm2a*, signature genes of positive  
233 selection<sup>46</sup>. Based on this profile we define cells from these clusters as maturing  $\alpha\beta$  T  
234 cells.

235 Importantly, nearly all cells associated with the maturing  $\alpha\beta$  or  $\gamma\delta$  T cell clusters  
236 were non-cycling (Fig 4B), and therefore, not ‘true’ DN4 cells. Retroviral transduction  
237 depends on cell being cycling<sup>47</sup>. Therefore, we determined whether ‘true’ DN4 cells  
238 could be separated from contaminating populations *ex vivo* with retroviruses. Virally  
239 transduced or non-transduced DN4 cells were placed in OP9-DL1 culture. Non-  
240 transduced DN4 cells preferentially give rise to single-positive cells expressing high  
241 levels of surface TCR, whereas, transduced DN4 become DP (Fig 4F-G). Since OP9-  
242 DL1 cells are unable to support positive selection, we conclude that these non-  
243 transduced DN4 cells are post-positive selection cells transitioning to SP. Together,  
244 these results demonstrate that the phenotypically defined DN4 compartment is  
245 heterogenous and establishes retroviral transduction as a method to isolate DN4 cells  
246 for *in vitro* analysis.

247

248 Ankle2 is a critical Zfp335-regulated gene required for survival of DN4 thymocytes

249         Next, we focused our scRNA-seq analyses on determining the transcriptional  
250 changes in DN4 cells resulting from loss of Zfp335. Maturing  $\alpha\beta$  and  $\gamma\delta$  cells were  
251 removed leaving only 'true' DN4 cells. Based on recombination kinetics (Supp Fig 1D)  
252 not all Zfp335cKO DN4 cells have undergone deletion. *Zfp335* expression could not  
253 reliably delineate mutant from non-mutant cells due to low detection rate (5.6% of  
254 Zfp335cKO vs 12.8% of WT cells). To identify true mutant DN4 cells in our dataset, we  
255 assessed transcription factor activity. Gene set scores were calculated for each cell  
256 based on the expression of the Zfp335 ChIP-seq target genes down-regulated in mutant  
257 DP cells (Fig 1J,K). Zfp335cKO cells exhibited a bimodal distribution for the gene set.  
258 Using established methods<sup>48</sup>, cutoff values were determined and cells falling below this  
259 threshold were considered true mutants (Supp Fig 5A). Cutoffs were confirmed by  
260 differential expression analysis between WT and Zfp335cKO targets high or Zfp335cKO  
261 targets low cells. Compared to WT, Zfp335cKO targets low cells exhibited differential  
262 expression of 80 genes (60 down, 20 up; Supp Fig 4B) whereas Zfp335cKO targets  
263 high cells only exhibited differential expression of 7 genes (5 down, 2 up; Supp Fig 4C).

264         Zfp335cKO cells above the threshold were considered non-mutant, removed and  
265 the remaining cells were then reanalyzed (Fig 5A) identifying 8 unique clusters (Supp  
266 Fig 4D). WT and mutant cells were distributed across each cluster. C1-3 were enriched  
267 for WT whereas C4 was almost entirely mutant cells (Supp Fig 4E). Despite regression  
268 of standard cell cycle-associated genes, clustering was largely dictated by cell cycle  
269 (Supp Fig 4F-I). We observed no differences in cell cycle phase distributions between

270 WT and mutant (Supp Fig 4H). Therefore, we chose to compare WT and mutant DN4  
271 cells based on genotype. Among the 60 down-regulated genes in mutant DN4 cells, 44  
272 are Zfp335 targets by ChIP-seq (Fig 5B)<sup>42</sup>. We hypothesized that reduced expression of  
273 one or more of these genes was responsible for the increased rates of apoptosis  
274 observed in mutant DN4 cells. Thus, we examined expression of the 12 Zfp335 target  
275 genes with experimental evidence demonstrating a negative regulatory role in cell death  
276 (Fig 5C-D). Four exhibited reduced expression in mutant DN4 thymocytes (Fig 5C).  
277 Examination of expression frequency identified *Ankle2* to have the greatest reduction in  
278 percent of mutant cells expression (Fig 5E).

279 *Ankle2* encodes an ER-restricted ankyrin repeat and LEM domain-containing  
280 protein<sup>49</sup>. *Ankle2* was recently identified as a critical Zfp335-regulated factor in the  
281 establishment of the naïve T cell<sup>42</sup>. Therefore, we tested whether *Ankle2*  
282 overexpression could rescue Zfp335cKO apoptosis. WT or Zfp335cKO DN3 thymocytes  
283 were transduced with EV or *Ankle2* retrovirus and cultured on OP9-DL1 cells.  
284 Importantly, *Ankle2* overexpression was able to fully rescue Zfp335-deficient  
285 thymocytes from increased rates of apoptosis (Fig 5F-G). Moreover, *Ankle2*  
286 overexpression led to significantly increased proportions of DP cells among Zfp335cKO  
287 samples (Fig 5H).

288 Next, we sought to confirm that *Ankle2* expression is directly regulated by Zfp335  
289 in pre-T cells. Analysis of published ChIP-seq data showed Zfp335 binds the proximal  
290 promoter of *Ankle2* in thymocytes (Fig 5I). To examine the relationship between *Zfp335*  
291 and *Ankle2* expression we utilize the DN4-like mouse thymocyte cell line *Scid.adh.2c2*<sup>50</sup>  
292 for CRISPR-based transcriptional inhibition (CRISPRi) studies<sup>51</sup>. These cells were

293 transduced with retroviruses expressing *Zfp335* promoter-targeting gRNA and anti-  
294 GCN4scFv-sfGFP-KRAB fusion construct. *Zfp335*-targeted cells exhibited reduced  
295 *Ankle2* expression proportional to the efficiency of *Zfp335* knock-down (KD) (Fig 5J).  
296 Additionally, *Zfp335*KD resulted in increased expression of *Bax* like that observed in  
297 *Zfp335*cKO thymocytes (Fig. 5K). Together, these results demonstrate a direct  
298 relationship between *Zfp335* and *Ankle2* expression in developing T cells and suggest  
299 reduced *Ankle2* expression resulting from loss of *Zfp335* drives DN4 apoptosis in  
300 *Zfp335*cKO mice.

301

302 Disruption of the *Zfp335*/*Ankle2*/*Baf* axis drives cGAS/STING-dependent apoptosis of  
303 DN4 thymocytes

304 Next, we sought to determine the mechanism driving this increase in cell death  
305 resulting from reduced *Ankle2* expression. *Ankle2* has previously been shown to control  
306 nuclear envelope (NE) reassembly and integrity following mitosis through regulation of  
307 Barrier to Autointegration Factor 1 (*Banf1*) phosphorylation. Indeed, disruption of  
308 *ANKLE2* or *BANF1* expression via siRNA knockdown in Hela cells led to severe  
309 disruptions in NE architecture (Supp Fig 6A).

310 Accumulation of cytosolic DNA or exposure of nuclear contents to the cytosol via  
311 NE disruption have been shown to activate the cGAS/STING pathway<sup>36, 52</sup>. In T cells,  
312 cGAS/STING signaling generally results in anti-proliferative and pro-apoptotic effects<sup>30,</sup>  
313 <sup>31, 33, 53</sup>. Therefore, we hypothesized that NE defects resulting from disruption of the  
314 *Ankle2*-*Banf1* pathway downstream of *Zfp335* loss drives cGAS/STING activation.  
315 Consistent with this hypothesis, GSEA revealed an enrichment for genes upregulated

316 by T cells in response to STING signaling in both our bulk DP and single-cell DN4  
317 datasets (Fig 6A-B). Additionally, we found increased IRF3 activity among mutant cells  
318 (Fig 6C). cGAS/STING-mediated death of mature T cells occurs in part, due to  
319 increased expression of pro-apoptotic Bcl2 family genes<sup>31</sup>. Like our findings from bulk  
320 RNA-seq (Fig 4A), we also observed increased expression of Bbc3 (PUMA), Pmaip1  
321 (NOXA), Bcl2l11 (Bid) and Bax among Zfp335cKO DN4 cells in our scRNA-seq dataset  
322 (Fig 6D).

323 In addition to nuclear DNA, mitochondrial DNA (mtDNA) serves as a substrate for  
324 cGAS<sup>54</sup>. mtDNA release requires mitochondrial outer membrane permeabilization  
325 resulting in mitochondrial membrane depolarization<sup>55</sup>. Examination of mitochondria  
326 showed Zfp335cKO thymocytes exhibit normal mitochondrial membrane potential and  
327 total mitochondrial mass (Supp Fig 6B-C). Therefore, mtDNA release is unlikely to be  
328 driving cGAS/STING-mediated death following loss of Zfp335. Instead, exposure of  
329 gDNA to cytosolic cGAS resulting from disrupted nuclear envelope architecture is the  
330 most likely cause.

331 To test the contribution of cGAS/STING to increased rates of DN4 apoptosis in  
332 Zfp335cKO mice 'true' DN4 cells were isolated by EV viral transduction then placed in  
333 OP9-DL1 culture for 3 days with cGAS (RU.521)<sup>56</sup> or STING (H-151)<sup>57</sup> inhibitors.  
334 Chemical inhibition of either cGAS or STING fully rescued Zfp335cKO DN4 cells from  
335 death (Fig 6E). Additionally, Zfp335cKO mice receiving H-151 for 7 days exhibited  
336 significantly increased numbers of total thymocytes compared to vehicle controls (Fig  
337 6F). Importantly, this increase in cellularity was primarily due to increased DP numbers  
338 (Fig 6F-J). Due to the short duration of treatment, we conclude that the increase in DP

339 cells among H-151-treated *Zfp335*cKO mice is the result of reduced cell death during  
340 the preceding proliferative DN4.

341 Next, we sought to determine the role of the *Zfp335*/*Ankle2*/*Baf* axis in  
342 suppressing the cGAS/STING-mediated apoptosis in DN4 cells. To test this, *R26<sup>LSL-Cas9</sup>*  
343 *Tcrd<sup>CreERT2</sup>* DN3/DN4 thymocytes<sup>58</sup> were transduced with retroviruses expressing  
344 *Zfp335*, *Ankle2*, or *Banf1* (encoding Baf) and *Mb21d1* (encoding cGAS) or *Tmem173*  
345 (encoding STING)-targeting gRNAs or non-targeting control gRNAs (NTG) then cultured  
346 for three days with OP9-DL1 cells in the presence of 4-hydroxytamoxifen. Consistent  
347 with conditional deletion, Cas9 targeting of *Zfp335* lead to a substantial increase in DN4  
348 apoptosis (Fig 6K-L). Additionally, targeting of *Ankle2* or *Banf1* similarly lead to  
349 increased DN4 apoptosis. Importantly, these increases in apoptosis were cGAS/STING-  
350 dependent (Fig 6K-L). Similar results were observed when Cas9 expression was  
351 controlled by E8<sub>III</sub>-cre (Supp Fig 6D-E). Together, these results demonstrate that  
352 disruption of the *Zfp335*/*Ankle2*/*Baf* axis drives cGAS/STING-mediated apoptosis of  
353 post- $\beta$ -selection DN4 thymocytes.

354

#### 355 DN4 thymocytes are uniquely sensitive to cGAS/STING-mediated cell death

356 Finally, we sought to determine whether sensitivity to cGAS/STING-driven cell  
357 death is a unique feature of *Zfp335*cKO DN4 cells or a mechanism of the DN4 stage.  
358 DN-enriched WT thymocytes were treated with the STING agonist cridanimod (CMA)  
359 overnight then assayed for apoptosis. Interestingly, we found DN4 cells are uniquely  
360 sensitive to STING-mediated apoptosis (Fig 6M-N). Additionally, viability of *Zfp335*cKO  
361 *Bcl2*-Tg thymocytes was not impacted by CMA treatment (Fig 6O) suggesting that



362 induction of pro-apoptotic Bcl2 family members downstream of STING activation are  
363 necessary for apoptosis of DN4 thymocytes.

364 Together, these data demonstrate that activation of the cGAS/STING pathway is  
365 a major contributor to Zfp335cKO DN4 apoptosis and that WT DN4 cells are uniquely  
366 sensitive to cGAS/STING-mediated death. Altogether, our studies demonstrate that loss  
367 of Zfp335 leads to defective T cell development resulting from dysregulation of the  
368 Zfp335/Ankle2/Baf axis ultimately driving cGAS/STING-mediated DN4 cell death.

369

## 370 Discussion

371 In this study, we identify Zfp335 as a critical transcription factor regulating early T  
372 cell development within the thymus. Specifically, it functions to promote survival of  
373 proliferating cells following  $\beta$ -selection. Conditional deletion of Zfp335 led to severe  
374 reductions in all T cell populations beginning at the DN4 stage of development.  
375 Mechanistically, we show that reduced expression of the Zfp335-regulated gene Ankle2  
376 is responsible for increased sensitivity to cell death and Ankle2 regulates nuclear  
377 envelope architecture. Additionally, the increased rates of thymocyte death resulting  
378 from loss of Zfp335 occurs through a cGAS/STING-dependent mechanism.

379 Our studies provide for the first a comprehensive assessment of the  
380 heterogeneity within the DN4 thymocyte compartment at the single cell level.  
381 Surprisingly, phenotypically defined DN4 cells consist of cycling cells expressing pre-T $\alpha$   
382 which represent 'true' DN4 cells and mature or maturing  $\alpha\beta$  and  $\gamma\delta$  T cells. The cells we  
383 identified expressing TCR $\alpha$  transcripts exhibited expression patterns consistent with

384 positive selection<sup>46</sup> and therefore, are likely post positive-selection cells which have  
385 transiently lost surface expression of TCR, CD4 and CD8. It is known that positive  
386 selection induces a slight and transient down-regulation of CD4 and CD8<sup>59</sup>, however,  
387 these maturing  $\alpha\beta$  cells identified in our dataset seem to have completely lost both  
388 protein and mRNA expression. Alternatively, these cells may have undergone positive  
389 selection without ever expressing CD4 or CD8. Regardless, these maturing cells may  
390 represent a novel developmental path within the thymus. However, more detailed  
391 studies will be needed to fully characterize these cells to determine if they represent a  
392 unique lineage or simply a rare differentiation path that can be taken by any positively  
393 selected cell.

394 Han *et al.* recently identified a hypomorph allele of *Zfp335* (*Zfp335<sup>bloto</sup>*) as the  
395 causative mutation led to reduced total peripheral T cells and an almost complete  
396 absence of naïve T cells. They found *Ankle2* to be a critical *Zfp335*-regulated gene  
397 controlling late stages of T cell development. However, the mechanism by which *Ankle2*  
398 regulates maturation, and the establishment of the naïve T cell compartment remains  
399 unclear. The lack of apparent developmental defects in *Zfp335<sup>blt/blt</sup>* mice during early T  
400 cell development is likely due to their use of a hypomorph allele instead of a conditional  
401 knock out as *Zfp335<sup>blt/blt</sup>* mice exhibited normal expression of *Ankle2* during the DN4  
402 stage.

403 We have shown that *Zfp335* is at least partially regulated by E protein activity in  
404 developing T cells. E proteins play numerous indispensable roles throughout organismal  
405 development, including T cell development <sup>4, 22, 37, 38, 39, 40, 60, 61, 62</sup>. However, due to  
406 widespread binding throughout the genome, the roles for transcriptional networks

407 established by E proteins remain incompletely understood<sup>40</sup>. Our studies identify Zfp335  
408 as a novel transcription factor downstream of E proteins critical to T cell development.

409 To date, studies of T cell-intrinsic roles for cGAS/STING pathway have largely  
410 focused on activation via synthetic STING agonists. These studies have exclusively  
411 focused on roles of this pathway in mature peripheral T cells. To our knowledge, this is  
412 the first report of a physiological role for cGAS/STING in T cell development.  
413 Additionally, our identification of the Zfp335/Ankle2/Baf axis as key in repression of  
414 cGAS is the first transcriptional pathway identified which functions to control cGAS  
415 activation.

416 Baf itself was recently identified as a key inhibitor of cGAS sensing of self-DNA  
417 through competitive binding. The ability of Baf to bind DNA is dependent upon its  
418 dephosphorylation which has been shown to be controlled by Ankle2 during mitotic exit.  
419 Therefore, we propose the following mechanism by which loss of Zfp335 drives  
420 cGAS/STING-mediated apoptosis of DN4 thymocytes. Loss of Zfp335 results in  
421 impaired Ankle2 expression which in turn leads to the failure of Baf dephosphorylation  
422 during division. Baf hyperphosphorylation leads to improper NE reassembly and can  
423 drive spontaneous NE rupture exposing nuclear DNA to the cytosol allowing  
424 unrestricted cGAS activation.

425 Interestingly, in humans, ANKLE2 is a target of Zika virus protein NS4A which  
426 antagonizes its activity ultimately leading to microcephaly<sup>63</sup>. Humans carrying  
427 homozygous or compound heterozygous mutations in either ZNF335 or ANKLE2 exhibit  
428 severe microcephaly like that seen in Zika patients<sup>34, 64</sup>. Recent studies have  
429 demonstrated a critical role for central nervous system immune cells in regulating

430 neuronal stem cell maintenance and differentiation. Specifically, microglia play a key  
431 role in this process<sup>65, 66, 67</sup>. Under conditions which stimulate cGAS activity, microglia  
432 and other CNS immune cells preferentially undergo apoptosis<sup>68</sup>. Based on the  
433 mechanism revealed in this study it is possible that microcephaly resulting from Zika  
434 infection or loss of ZNF335 or ANKLE2 may be driven by cGAS/STING-dependent  
435 apoptosis of neuronal progenitors and/ or CNS immune cells. Should our mechanism  
436 extend to neuronal progenitors or CNS immune cells it may be possible to  
437 pharmaceutically prevent microcephaly in these specific instances by inhibition of the  
438 cGAS/STING pathway. However, further research will be required to determine the  
439 viability of such a therapeutic approach.

#### 440 **Acknowledgements**

441 This study was funded by the NIH (R01-GM059638 and P01-AI102853) to YZ and (P01-  
442 AI102853) to DW.

443 We thank M. Cook, N. Martin, B. Li and L. Martinek (Duke University Cancer Institute  
444 Flow Cytometry Core) for technical support and cell sorting. We thank the Duke  
445 Molecular Physiology Institute for preparation of scRNA-seq libraries. We thank M.  
446 Krangel, QJ Li, J. Racine, D. Serreze, and M. Hasham for critical reading and  
447 comments on the manuscript. We thank M. Ciofani and J. Park for providing cell lines  
448 and mice. We thank M. Parker and J. Wheaton of M. Ciofani's lab for providing MSCV-  
449 Thy1.1 and MSCV-sgRNA expression vectors.

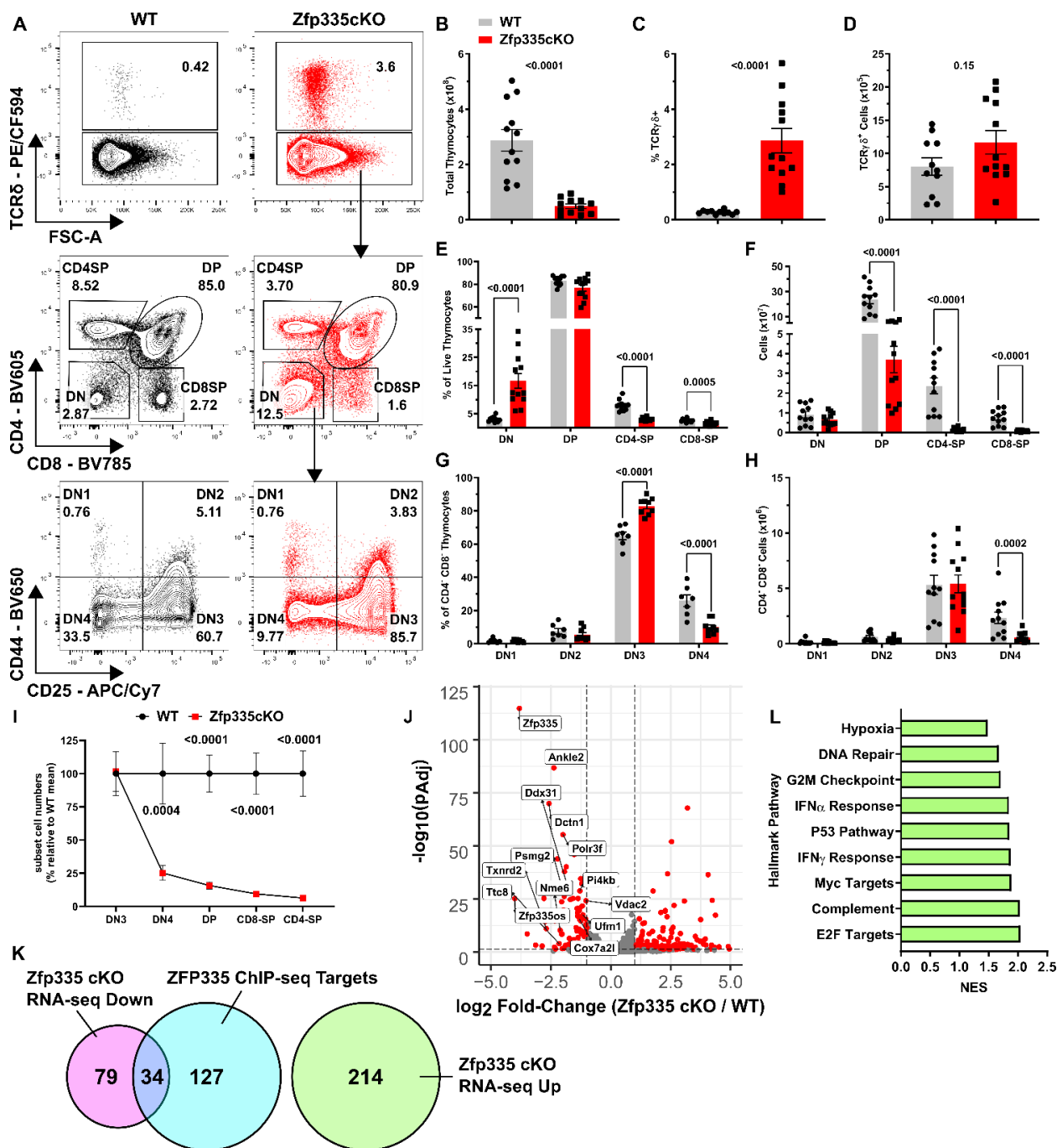
#### 450 **Author Contributions**

451 JJR, YZ and DW designed experiments and analyzed and interpreted data. JJR, QW,  
452 NM, DD, MJH, SW, SR and AVC performed experiments. JJR, YZ and DW wrote the  
453 manuscript with editing by the co-authors. JJR and YZ oversaw and supervised all  
454 aspects of the study.

455 **Declaration of interests**

456 The authors declare no competing interests.

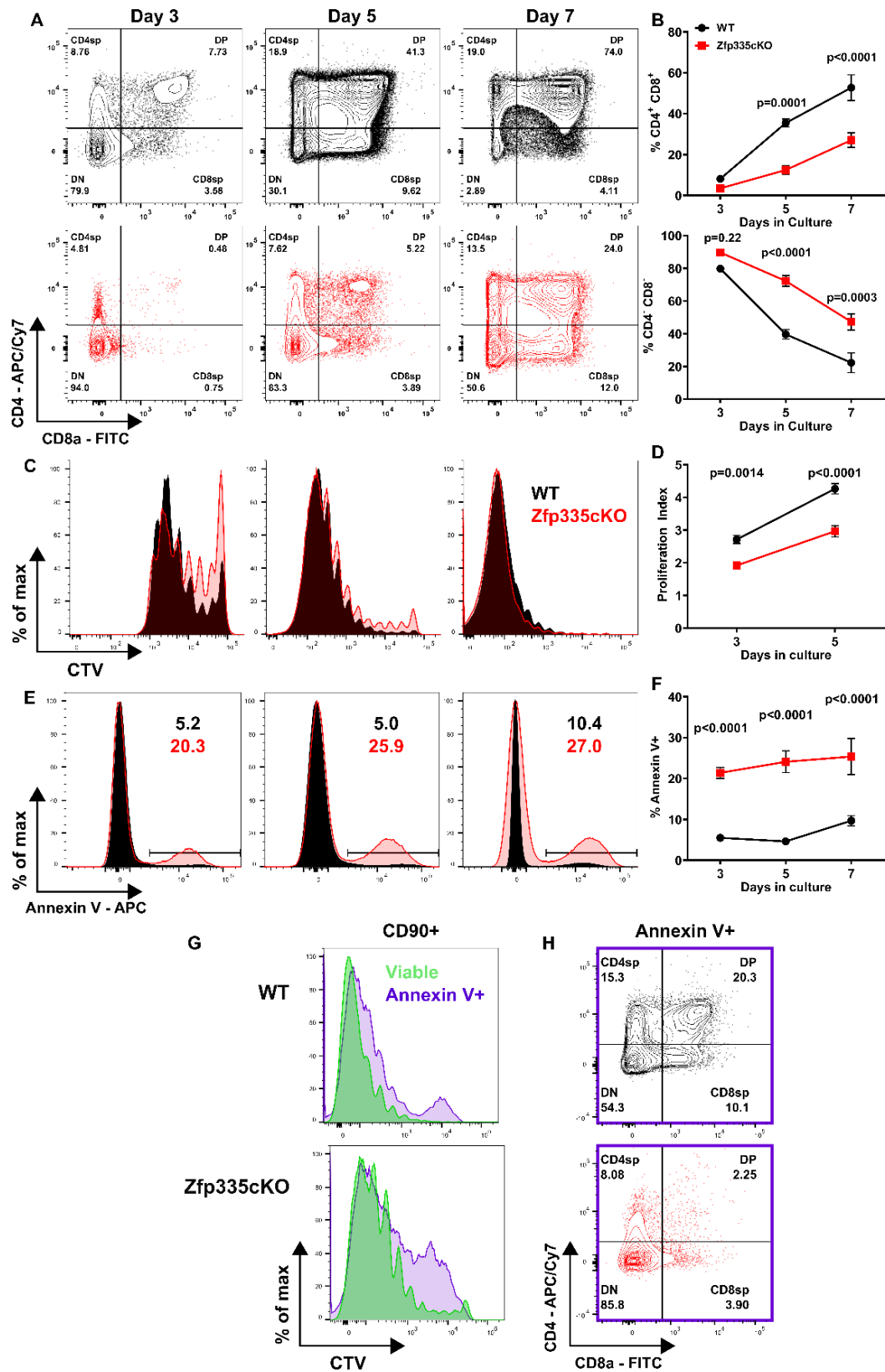
457 **Figures**



458

459 **Figure 1 – Zfp335 is critical to  $\alpha\beta$  T cell development.** (A) Gating schema for ex vivo analysis  
 460 thymocyte development beginning with live thymocytes (DAPI $^-$  CD90.2 $^+$ , gating not shown). (B)  
 461 Total thymic cellularity in WT (Cre-negative) or *Zfp335<sup>fl/fl</sup> E8iii-cre* (Zfp335 cKO) mice. Total  
 462 numbers (C) and frequency (D) of TCR $\gamma\delta^+$  cells in WT or Zfp335 cKO thymuses. Numbers (E)  
 463 and frequencies (F) of DN, DP, and SP thymocyte subsets in WT or Zfp335 cKO thymuses.  
 464 Numbers (G) and frequencies (H) of early DN1-DN4 thymocyte subsets in WT or Zfp335 cKO  
 465 thymuses. (I) Relative cells numbers in DN3-SP thymocyte subsets represented as percent of  
 466 WT mean. (J) Differential expression of select Zfp335-target genes by RNA-seq. (K) Overlap  
 467 between Zfp335 ChIP-seq (GSE58293) and differentially expressed genes in Zfp335 cKO and

468 WT DP. (L) Gene Set Enrichment Analysis of differentially expressed genes (K). Positive  
469 enrichment scores indicate pathways positively enriched in Zfp335 cKO cells. (A-K) Cre-  
470 negative WT (n=11) and Zfp335 cKO (n=12) 4-5-week-old male and female mice from four  
471 independent experiments. *P*-values determined by Two-way ANOVA with *post hoc* Sidak test.  
472 (I-K) RNA-seq analysis of *Zfp335*<sup>+/+</sup> *E8III-cre* or Zfp335 cKO DP thymocytes (n=3 each) of 6  
473 week old female mice from one experiment.



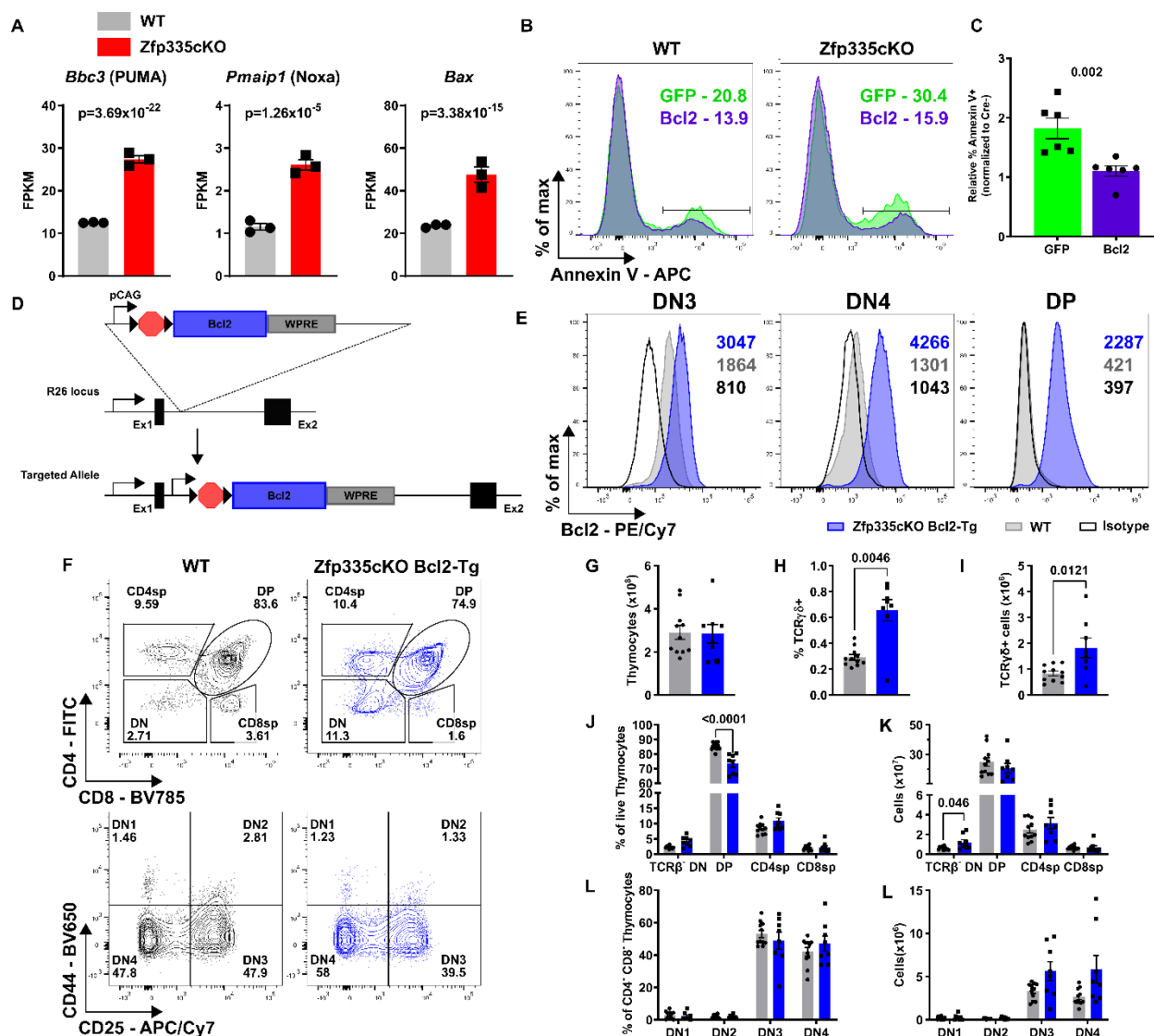
474

475 **Figure 2 - Zfp335cKO DN4 thymocytes undergo increased rates of apoptosis. (A-B)**  
 476 Assessment of developmental progression throughout OP9-DL1 culture. Proliferation



477 assessment (C-D) by Cell Trace Violet (CTV) dilution and apoptosis analysis (E-F) based on  
 478 Annexin V binding at day3, 5 or 7 of culture. (G) Representative comparison of CTV dilution  
 479 between Annexin V<sup>+</sup> and viable (DAPI<sup>-</sup> Annexin V<sup>-</sup>) cells on day 5 of culture. Representative  
 480 CD4 vs CD8 expression among Annexin V<sup>+</sup> cells on day 5 of culture. n=6 WT or n=5  
 481 Zfp335cKO from three independent experiments. P-values determined using Two-way  
 482 Repeated Measures ANOVA with *post hoc* Sidak Test. Plots show mean  $\pm$  sem.

483

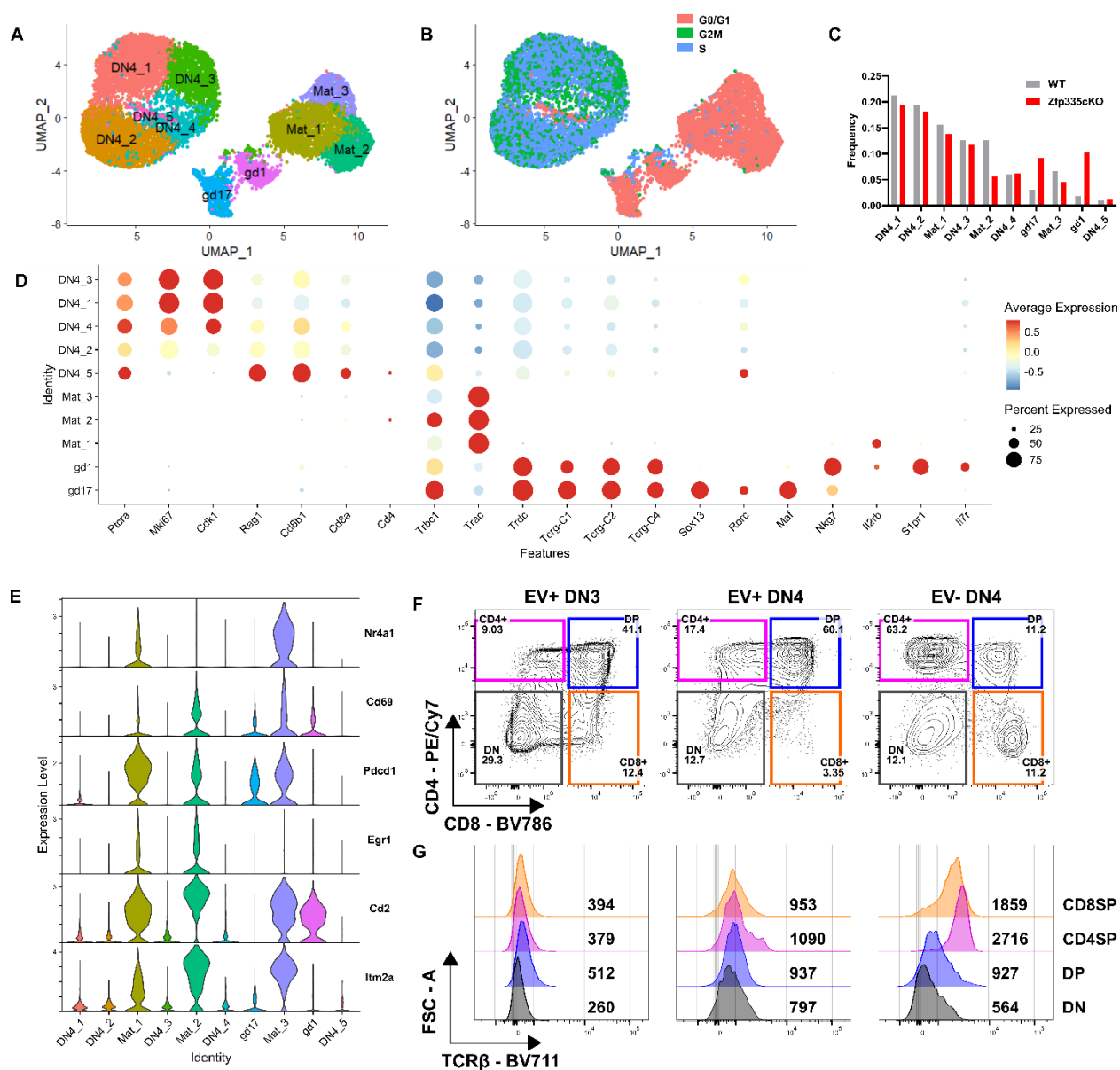


484

485 **Figure 3 – Bcl2 overexpression rescues Zfp335-deficient thymocytes from apoptosis.** (A)  
 486 Expression of pro-apoptotic Bcl2 family genes *Bbc3*, *Pmaip1*, or *Bax* from RNA-seq of control or  
 487 *Zfp335<sup>fl/fl</sup> E8III-cre* DP thymocytes. Representative gating (B) and quantification of apoptosis  
 488 among *Zfp335<sup>fl/fl</sup> E8III-cre* thymocytes transduced with Bcl2 or GFP RV after 5 days of OP9-DL1  
 489 culture (n=5). (E) Representative expression of isotype control (open black) or Bcl2 in WT (grey)  
 490 or *Zfp335<sup>fl/fl</sup> R26<sup>LSL-Bcl2</sup> E8III-cre* (blue) DN3, DN4 or DP thymocytes. (F) Gating for identification  
 491 of thymocyte subsets in WT WT (grey) or *Zfp335<sup>fl/fl</sup> R26<sup>LSL-Bcl2</sup> E8III-cre* (blue) mice. DN1-4 gating  
 492 pre-gated on TCR $\beta$ . (G) Total thymocyte numbers. Total numbers (H) and proportions (I) of

493 TCR $\delta^+$  cells. Frequencies (J) and total numbers (K) of DN, DP, CD4-SP and CD8-SP  
 494 thymocytes. Frequencies (L) and total numbers (M) of DN1-DN4 thymocytes. (F-M) n=11 WT or  
 495 n=8 *Zfp335<sup>fl/fl</sup> R26<sup>LSL-Bcl2</sup> E8III-cre*. Data compiled from one (A), two (B-C) or five (D-L)  
 496 independent experiments. P-values determined by Wald test (A), Mann-Whitney U-test (C) or  
 497 Two-way ANOVA with *post hoc* Sidak's test (H-M). Plots show mean  $\pm$  sem.

498

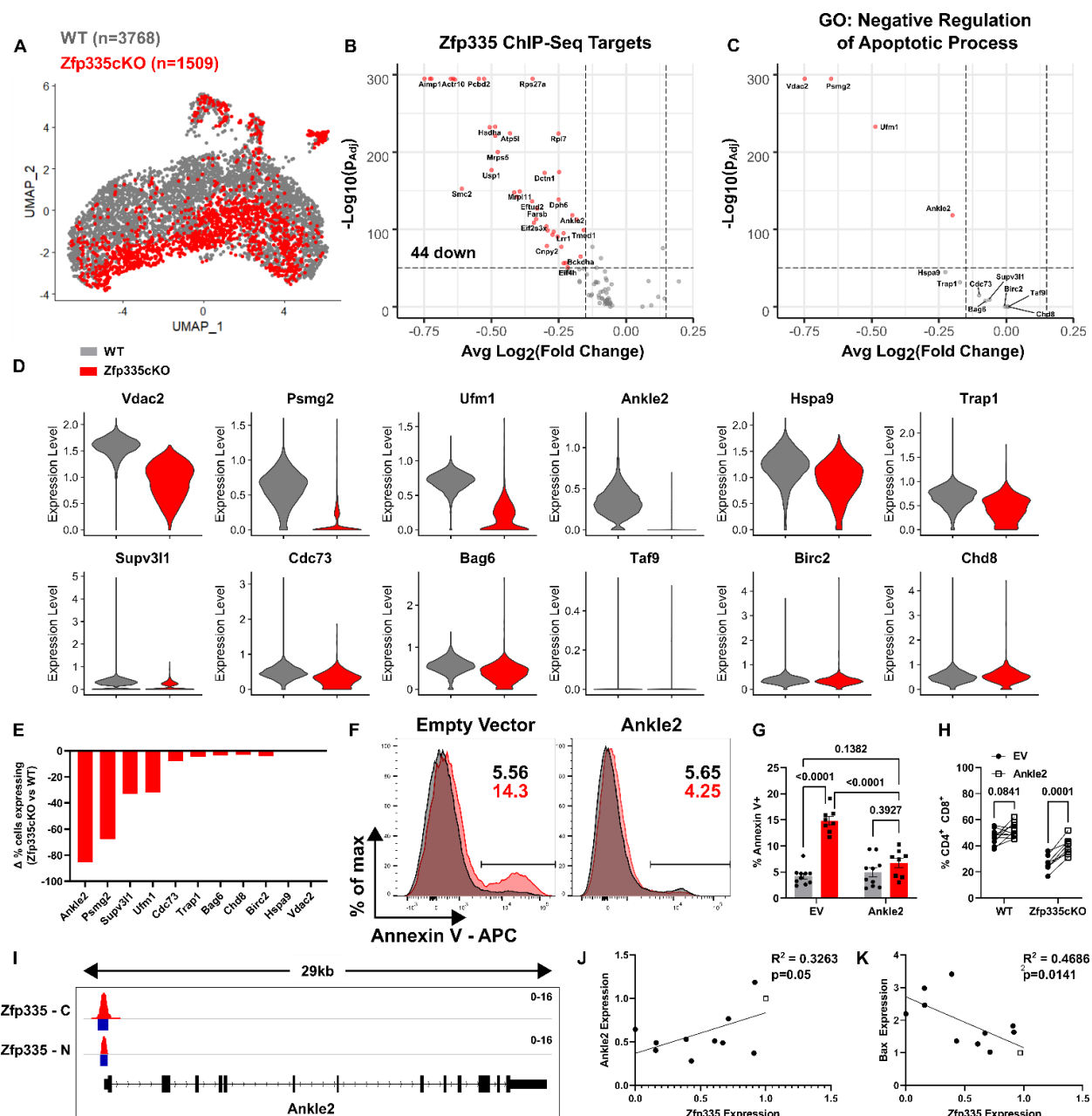


499

500 **Figure 4 – Defining the ‘true’ DN4 thymocyte population at the single cell level.** (A) UMAP  
 501 projection and identification of 10 clusters identified in full scRNA-seq dataset. (B) UMAP  
 502 colored by cell cycle phase. Blue or green identify actively cycling cells. (C) Frequency  
 503 distributions for WT (n=6357) and *Zfp335cKO* (n=5392) cells across the ten clusters. (D)  
 504 dot plot of key cell type-defining genes. (E) Violin plots of positive selection signature genes in  
 505 thymocytes (Mingueneau et al. 2013). (F) Representative gating for CD4 vs. CD8 expression on

506 day 3 of OP9-DL1 cultures seeded with WT Thy1.1 retrovirus transduced (EV+) DN3 or DN4  
 507 cells or non-transduced (EV-) DN4 cells. (G) Representative TCR $\beta$  expression among DN, DP,  
 508 CD4SP or CD8SP cells from (F). Numbers indicate geometric MFI of TCR $\beta$  expression. (F-G)  
 509 Data representative of two independent experiments.

510

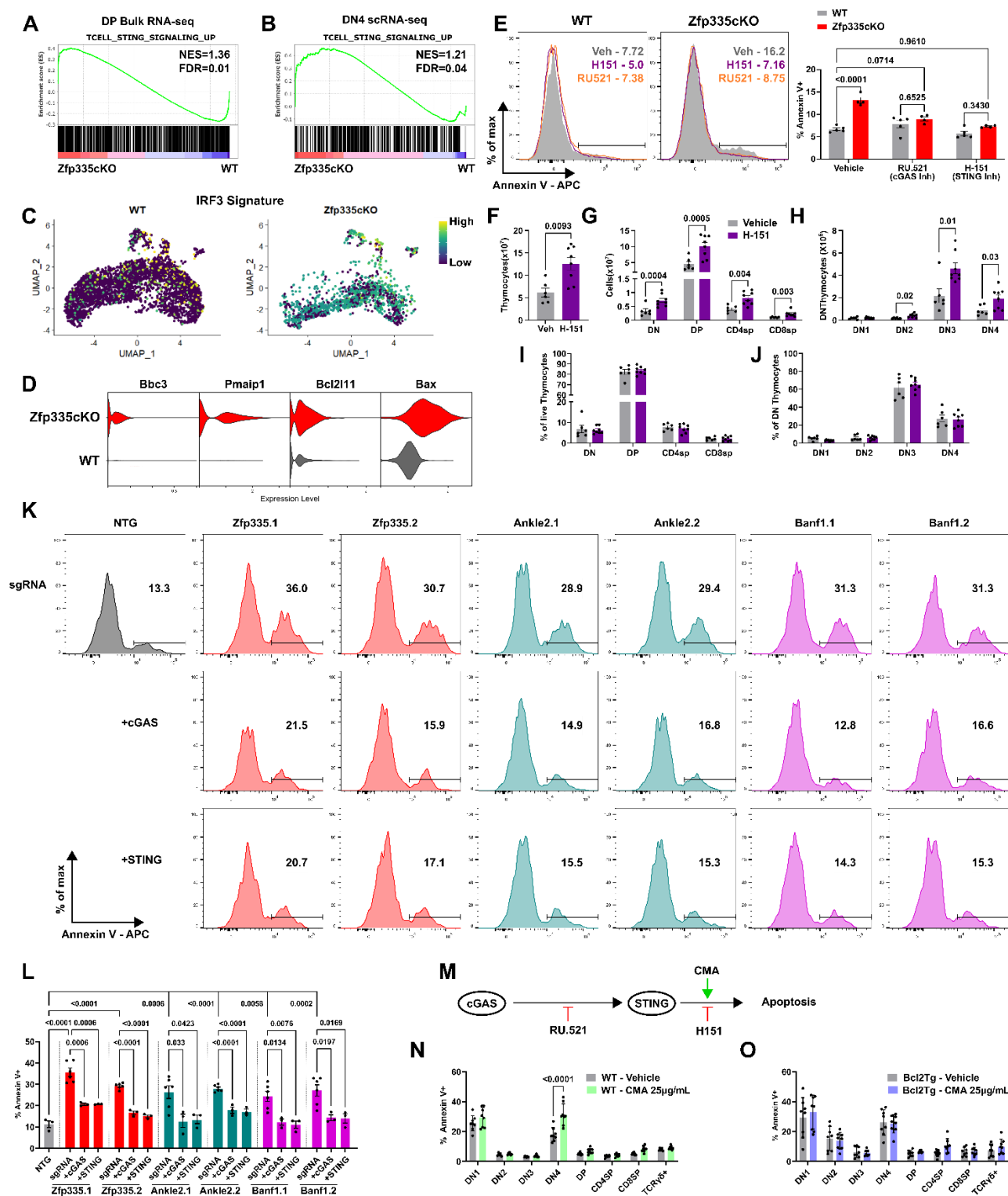


511

512 **Figure 5 – scRNA-seq identifies Ankle2 as a critical Zfp335-regulated gene controlling**  
 513 **survival of DN4 thymocytes.** (A) Violin plot of gene set score for Zfp335 target genes down-  
 514 regulated in mutant DP thymocytes (Fig 1L-M) and cutoff value used to identify true Zfp335  
 515 mutant cells (black box). (B) UMAP projections colored by genotype. Volcano plot of all  
 516 differentially expressed Zfp335 target genes (C) or those experimentally shown negatively

517 regulate apoptotic processes (D) between Zfp335 mutant and WT cells. (E) Violin plots of anti-  
518 apoptotic Zfp335 target gene expression between Zfp335 mutant and WT DN4 cells. (F)  
519 Differential proportions of Zfp335 mutant cells expressing anti-apoptotic genes from E compared  
520 to WT cells. Representative gating (F) and quantification of apoptosis (G) or DP cell frequency  
521 (H) for EV or Ankle2 retrovirus transduced WT (n=10) or Zfp335cKO (n=8) DN3 thymocytes  
522 cultured on OP9-DL1 cells for 3 days. (I) Zfp335 ChIP-seq track of *Ankle2* locus in WT  
523 thymocytes (Zfp335-C or Zfp335-N antibodies, GSE58293). Blue boxes indicate significant  
524 binding peaks. Correlation between Ankle2 (J) or Bax (K) and Zfp335 expression in  
525 Scid.adh.2c2.SunTag CRISPRi cells expressing non-targeting (open squares) or Zfp335-  
526 targeting (closed circles) gRNAs. Data are compiled from one (A-E), two (J-K) or three (F-H)  
527 independent experiments. *P*-values determined by Wilcoxon Rank Sum test (B-C), two-way  
528 ANOVA with *post hoc* Tukey's test for multiple comparisons (G), repeated measures ANOVA  
529 with Sidak's test (H) or simple linear regression (J-K). Plots show mean  $\pm$  sem.

530



531

532 **Figure 6 – The Zfp335/Ankle2/Baf axis suppresses cGAS/STING-mediated apoptosis of**  
 533 **DN4 thymocytes.** GSEA enrichment plots for T cell-specific STING signaling gene signature in  
 534 DP bulk (A) or DN4 scRNA-seq data sets (B). (C) UMAP projection of IRF3 gene signature in  
 535 WT or Zfp335 mutant DN4 thymocytes. (D) Violin plots of pro-apoptotic Bcl2 gene expression in  
 536 WT or Zfp335 mutant DN4 thymocytes. (E) Representative histograms and quantification of

537 Annexin V-binding for WT or Zfp335cKO DN4 thymocytes treated with cGAS (RU.521) or STING  
538 (H-151) inhibitors or vehicle control and cultured on OP9-DL1 stromal cells for three days. Total  
539 thymocyte (F), DN, DP, CD4SP and CD8SP (G) or DN1-DN4 cell numbers for Zfp335cKO mice  
540 treated with H-151 or vehicle *in vivo* for 7 days. (I-J) Thymocyte subset proportions for H-151 or  
541 vehicle treated Zfp335cKO mice. Representative gating (K) and quantification (L) of Annexin V  
542 binding among DN4 cells from  $R26^{LSL-Cas9} Tcrd^{CreERT2}$  thymocytes transduced with gRNA-  
543 expressing retroviruses and cultured for three days on OP9-DL1 cells with 4-hydroxytamoxifen.  
544 (M) Schematic diagram of inhibitors (RU.521 or H-151) or agonists (CMA) used to study  
545 cGAS/STING-dependent apoptosis of DN4 thymocytes. Percent apoptosis induced by small  
546 molecule activation of STING among WT (N) or Zfp335cKO Bcl2Tg (O) thymocyte subsets.  
547 Values calculated by subtracting % Annexin V+ of vehicle-treated from % Annexin V+ of STING  
548 agonist-treated for each sample. *P*-values determined by Mann Whitney U-test (F) or two-way  
549 ANOVA with *post hoc* Tukey's test (E) or Sidak's test (G-J,N-O) or one-way ANOVA with *post*  
550 *hoc* Tukey's test. Data shown are compiled from one (A-D), two (E), three (L-O) or five (F-J)  
551 independent experiments. Plots show mean  $\pm$  sem.

552

553

## 554 **Methods**

### 555 Mice

556 B6.Cg-Zfp335<sup>tm1Caw</sup> (Zfp335<sup>fl/fl</sup>, Stock No. 022413) and B6J.129(B6N)-  
557 *Gt(ROSA)26Sor<sup>tm1(CAG-cas9\*,-EGFP)Fevh/J</sup>* (R26<sup>LSL-Cas9</sup>, Stock No. 026175) mice were  
558 purchased from The Jackson Laboratory. C57BL/6J-Tg(Cd8a<sup>\*</sup>-cre)B6Asin (E8<sub>III</sub>-cre)  
559 mice were generously provided by Jung-Hyun Park (NIH). B6.129S-Tcrd<sup>tm1.1(cre/ERT2)Zhu</sup>  
560 (*Tcrd<sup>CreERT2</sup>*) have been maintained in our colony since original development. A modified  
561 Ai6 targeting vector to drive conditional overexpression of Bcl2 was generated by  
562 cloning in mouse *Bcl2* cDNA (Transomic Technologies) using FseI and SfiI restriction  
563 sites. R26<sup>LSL-Bcl2</sup> mice were generated by the Duke University Transgenic Facility using  
564 G4 mouse embryonic stem cells. Animals were maintained under specific pathogen-free  
565 conditions at the Cancer Center Isolation Facility of Duke University Medical Center. All  
566 experimental procedures were approved by the Institutional Animal Care and Use



567 Committee. All mice used in this study were 4-8 weeks old. For all experiments Cre-  
568 negative littermate controls were used unless otherwise stated.

### 569 Antibodies

570 All antibodies used in this study were purchased commercially and have previously  
571 been validated. Anti-TCR $\gamma\delta$  (GL3) was purchased from BD Biosciences. Anti- TCR $\gamma\delta$   
572 (GL3), rabbit anti-Lamin B (10H34L18) and goat anti-rabbit IgG (H+L)-Alexa Fluor 647  
573 were purchased from ThermoFisher Scientific. Anti-CD16/32 (2.4G2) was purchased  
574 from Tonbo Biosciences. Anti-CD90.1 (OX7), anti-CD90.2 (30-H12), anti-CD4 (RM4-5),  
575 anti-CD8 (53-6.7), anti-CD44 (IM7), anti-CD25 (PC61), anti-CD62L (MEL-14), anti-  
576 TCR $\beta$  (H57-597), anti-CD27 (LG.3A10), anti-Bcl2 (BCL/10C4), anti-CD24 (M1/69), anti-  
577 B220 (RA3-6B2), anti-CD11b (M1/70), anti-CD11c (N418), anti-CD19 (6D5), anti-  
578 Ly6G/Ly6C (RB6-8C5), anti-NK1.1 (PK136), anti-TER119 (TER-119), anti-CD117/c-kit  
579 (2B8), and Annexin V were purchased from Biolegend.

### 580 Flow cytometry and cell sorting

581 Thymus or spleen tissues were harvested from 4-8 week old mice. Tissues were then  
582 dissociated in FACS Buffer (PBS supplemented with 2.5% FBS and 2mM EDTA) using  
583 a Dounce Homogenizer and filtered through 70 $\mu$ m nylon mesh (Genesee Scientific) to  
584 yield single-cell suspensions. For spleen samples, red blood cells were lysed using 1x  
585 RBC lysis buffer then resuspended in FACS buffer. 0.5-1x10<sup>7</sup> cells were stained with  
586 fluorescently labelled antibodies for 30 minutes at 4°C then washed with excess FACS  
587 buffer. Prior to analysis propidium iodide (Sigma-Aldrich, Cat. P4170) or DAPI (Sigma-  
588 Aldrich, Cat. D9542) were added to a final concentration of 0.5 $\mu$ g/mL or 100ng/mL,

589 respectively for live/ dead discrimination. Cells were analyzed on a Fortessa X20 (BD  
590 Biosciences) or FACSCantoll (BD Biosciences) cytometer. For isolation of thymocyte  
591 subsets or virally transduced cells, sorting was performed using a FACSDiva (BD  
592 Biosciences) or Astrios (Beckman-Coulter) cell sorter. For sorting of thymocyte subsets  
593 *ex vivo*, staining included a lineage dump stain consisting of B220, CD11b, CD11c,  
594 CD19, GR-1, NK1.1, TCR $\beta$ , TCR $\gamma\delta$  and TER119 antibodies. All analyses were  
595 performed using FlowJo v10 software (TreeStar).

#### 596 Bulk RNA-seq

597 DP thymocytes (Lin<sup>-</sup> CD4<sup>+</sup> CD8<sup>+</sup>) were FACS sorted from total thymus of 7-week-old  
598 female Zfp335<sup>fl/fl</sup> E8<sup>III</sup>-cre or Zfp335<sup>+/+</sup> E8<sup>III</sup>-cre mice. Purified DP cells were lysed with  
599 Trizol and RNA isolated using the DirectZol Micro RNA prep kit (Zymo) according to  
600 manufacturer's recommended protocol. gDNA was eliminated by on-column DNase  
601 digestion. Libraries were prepared using standard preparation protocols by BGI  
602 Genomics. 150bp paired-end sequencing was performed on the BGISEQ-500  
603 sequencing platform.

604 Paired-end reads were mapped to the mouse mm10 reference genome using the  
605 HiSat2 software and count matrices generated using the featureCounts function of the  
606 Subreads software package. Differential expression analysis was performed using  
607 edgeR and DeSeq2 implemented through iDep.91  
608 (<http://bioinformatics.sdstate.edu/idep90/>). Gene-Set Enrichment Analysis (GSEA) was  
609 utilized to identify enriched pathways based on differential expression analysis using  
610 pre-ranked gene lists.



## 611 Cell Culture

612 OP9-DL1 cells, kindly provided by Maria Ciofani (Duke University) were cultured in  
613 MEM $\alpha$  (Gibco) supplemented with 10% FBS (Atlanta Biologicals) and 1x penicillin/  
614 streptomycin (Gibco). HEK293T cells were cultured in DMEM supplemented with 10%  
615 FBS, 1x penicillin/ streptomycin, 1x non-essential amino acids and 1x GlutaMAX. For  
616 OP9-DL1 culture of thymocytes, cultures were additionally supplemented with 5ng/mL  
617 recombinant mouse IL-7 (Biolegend). Scid.adh.2c2 cells were cultured in IMDM  
618 supplemented with 10% FBS (Hyclone), 1x penicillin/ streptomycin, 1x NEAA, 1x  
619 sodium pyruvate, 1x GlutaMAX, and 55 $\mu$ M  $\beta$ -mercaptoethanol. In some OP9-DL1  
620 cultures 5 $\mu$ g/mL RU.521 (Invivogen), 0.5 $\mu$ g/mL H-151 (Cayman Chemicals) or 20 $\mu$ g/mL  
621 Cridanimod (Cayman Chemicals) were added. All cultures were maintained at 37°C with  
622 5% CO<sub>2</sub>.

## 623 DN thymocyte enrichment

624 Total thymocytes were harvested from 4–8-week-old mice. Tissues were dissociated  
625 and strained through 30 $\mu$ m nylon mesh (Genesee Scientific). For purification of DN3/4  
626 thymocytes cells were stained with biotinylated antibodies against B220, CD3, CD4,  
627 CD8, CD11b, CD11c, CD19, CD44, c-Kit, GR-1, IgM, NK1.1, TCR $\beta$ , and TCR $\gamma\delta$ . For  
628 enrichment of total DN cells CD44 and c-Kit antibodies were excluded. Following  
629 antibody staining, cells were incubated with 50 $\mu$ L or 100 $\mu$ L of streptavidin magnetic  
630 particles (Spherotech, cat. SVM-40-100) / 10<sup>7</sup> cells at 2 x 10<sup>7</sup> cells/mL in FACS buffer  
631 for total DN enrichment or DN3/4 purification, respectively. Particle-bound cells were  
632 separated three times on a magnetic rack.

633 Retrovirus packaging and transduction

634 Retrovirus were generated by transfecting HEK293T cells with 1µg/mL each of MSCV  
635 transfer and pCL-Eco vectors using Lipofectamine 2000 (Invitrogen) or JetOptimus  
636 (Genesee Scientific) according to manufacturer's recommended protocols. Media was  
637 changed 24 hours post-transfection and viral supernatants harvested 24 hours later.  
638 DN3/4-enriched thymocytes were transduced with fresh viral supernatant via spinfection  
639 for 2 hours at 2300 rpm at 30°C with 6.7µg/mL polybrene (Millipore). Following  
640 spinfection cells were transferred to culture on OP9-DL1 stromal cells for overnight  
641 culture. 18-24 hours post-infection virally transduced (DsRed+ or Thy1.1+) DN3  
642 (CD25+) or DN4 (CD25-) were isolated by FACS sorting for an additional 3-5 days of  
643 culture in the OP9-DL1 culture system. For dual-targeting CRISPR experiments, equal  
644 volumes of sgRNA-Thy1.1 and -DsRed viral supernatants were mixed for transduction.

645 scRNA-seq library preparation

646 For single cell RNA-sequencing, DN4 thymocytes (Live Lin<sup>-</sup> CD4<sup>-</sup> CD8<sup>-</sup> CD25<sup>-</sup> CD44<sup>-</sup>)  
647 were sorted from one male and one female mouse pooled for each genotype using an  
648 Astrios Sorter. Sorted cells were encapsulated into droplets and libraries were prepared  
649 using a Chromium Single Cell 3' Kit using the v3.1 chemistry. 7,000 cells per genotype  
650 were targeted. scRNA-seq libraries were pooled and sequenced on a NovaSeq S Prime  
651 Flow Cell yielding an average depth of 71,584 or 67,816 reads per cells for Zfp335cKO  
652 or WT samples, respectively.

653 scRNA-seq analysis

654 scRNA-seq data were processed using the Cell Ranger pipeline (10x Genomics).  
655 FASTQ files were generated from raw base call logs (bcl2fastq, v2.20), aligned to the  
656 mouse mm10 (release 93) reference genome (cellranger, v3.1.0; STAR v2.5.3a) to  
657 generate raw gene count matrices.

658 All downstream analyses were performed using the R software package Seurat (v4.0.0).  
659 Data was filtered to exclude cells with < 1,000 genes detected or < 1,000 UMIs.  
660 Doublets were excluded by filtering cells with > 60,000 UMIs. Low-quality cells were  
661 further filtered by removal of cells with > 7.5% mitochondrial gene expression. Gene  
662 expression matrices were then merged, data normalized, scaled and cell cycle scored  
663 using standard methods with Seurat. Dropouts were imputed using the R package  
664 ALRA. Cell cycle phase was regressed, and principal component analysis (PCA) was  
665 performed on the 6,000 most variable genes. 35 principal components were selected for  
666 downstream analysis based on JackStraw analysis. Dimensionality reduction was  
667 performed by Uniform Manifold Approximation and Projection (UMAP) and clustering  
668 defined using a resolution of 0.5. Gene expression was visualized by VlnPlot, DotPlot  
669 and FeaturePlot functions in Seurat. Gene signature scores were calculated using  
670 SingleCellSignatureExplorer and previously described methods<sup>69</sup>. Differential  
671 expression analysis was performed using the FindMarkers function in Seurat with  
672 Wilcoxon Rank Sum Test.

### 673 Cloning cDNA overexpression vectors

674 Bcl2 overexpression vector was generated by cloning Bcl2 cDNA (Transomic  
675 Technologies, Cat. TCM1304) into the pMSCV-loxp-dsRed-loxP-eGFP-puro-WPRE  
676 vector (Addgene #32702) using the EcoRI and NsiI restriction sites. Ankle2 cDNA

677 (Transomic Technologies, Cat. TCM1004) was cloned into the MSCV-IRES-Thy1.1  
678 vector using NEBuilder Hifi Assembly (New England Biolabs). All vectors were  
679 propagated in Stbl3 cells (ThermoFisher Scientific).

#### 680 Generation of *Scid.adh.2c2-dCas9<sup>10x-GCN4</sup>* CRISPRi cells

681 dCas9<sup>10x-GCN4</sup> (pHRdSV40-dCas9-10xGCN4\_v4-P2A-BFP, Addgene #60904) was  
682 lentivirally transduced into *Scid.adh.2c2* cells, following which BFP+ cells were isolated  
683 by flow cytometry. Single cells were then cloned into 96 well plates and screened for  
684 knockdown efficiency using CD25 gRNA retroviral vectors. Clones exhibiting more than  
685 90% CD25 downmodulation were expanded for use in our studies.

#### 686 Generation of gRNA retroviral vectors

687 All gRNAs were designed using the CRISPick <sup>70</sup> gRNA design tool. All gRNAs were  
688 cloned into expression vectors by annealing followed by ligation into a BbsI cleavage  
689 site. The basic gRNA expression vector used was the MSCV-mU6-sgRNA-hPGK-  
690 Thy1.1 (kindly provided by Maria Ciofani). Knock-out gRNAs were first cloned into this  
691 Thy1.1 backbone. To generate DsRed expressing vectors for dual targeting, Thy1.1  
692 was removed by digestion with BamHI and EcoRI and replaced with DsRed Express II  
693 by NEBuilder Hifi Assembly. The CRISRPi retroviral vector was generated by first  
694 cloning the pSV40-scFv-GCN4-sfGFP-VP64-GB1-NLS (Addgene #60904) fusion  
695 construct into the MSCV-mU6-sgRNA-hPGK backbone followed by replacement of  
696 VP64 with KRAB using NEBuilder.

#### 697 qPCR analysis of gene expression

698 Following viral transduction, Scid.adh.2c2.dCas9<sup>10x-GCN4</sup> cells were assessed for  
699 transduction efficiency by flow cytometry. For samples exceeding 90% GFP+ 10<sup>6</sup> cells  
700 were lysed in Trizol and RNA isolated using the Direct-Zol MicroPrep kit. 500ng of RNA  
701 was reverse transcribed using SuperScript III Reverse Transcriptase (Invitrogen) with  
702 random hexamers according to the manufacturer's recommended protocol. 5ng of  
703 cDNA per 25µL reaction was then used for gene expression analysis with PowerTrack  
704 Sybr Green Master Mix (Applied Biosciences) according to the manufacturer's  
705 recommended protocol using fast cycling conditions with an Eppendorf MasterCycler  
706 qPCR machine. Relative expression was determined using the ddCt method with  
707 Gapdh being used for normalization.

#### 708 Determination of nuclear envelope structure

709 5x10<sup>4</sup> HeLa cells per well were reverse transfected with 15pmol siRNA using  
710 Lipofectamine RNAiMax (ThermoFisher Scientific) in an 8 well chamber slide according  
711 to recommended protocols. ANKLE2 and universal non-targeting control siRNAs were  
712 purchased from IDT (Design ID: hs.Ri.ANKLE2.13). BANF-targeting siRNAs were  
713 purchased from ThermoFisher Scientific (IDs: s16807, s16808, 26065). 48 hours post-  
714 transfection cells were fixed with 4% paraformaldehyde for 10 minutes at room  
715 temperature and permeabilized with permeabilization buffer for 1h at RT temperature.  
716 Primary antibody Lamin B (Invitrogen, Cat. 702972) were added for overnight incubation  
717 at 4C and washed with 1X PBS for three time. After that, secondary antibody Alexa  
718 Fluor 647-conjugated goat anti-rabbit antibody (Invitrogen, Cat. A32733) were added for  
719 12h at 4C in the dark. After washing with 1X PBS for three times, slides were mounted

720 with DAPI-containing mounting media (VECTORLAB, Cat. H-1200). Images were  
721 collected using Zeiss 780 upright confocal.

722 To analyze nuclear structure DAPI channel images were converted to binary with  
723 ImageJ. Following binarization, the Watershed function was used to separate touching  
724 cells. Circularity was then determined with a minimum threshold of 500 px<sup>2</sup>.

#### 725 *In vivo* H-151 treatment of mice

726 Mice were administered 750 pmol (210µg) of H-151 (Cayman Chemicals) or vehicle via  
727 intraperitoneal injection daily for 7 days beginning at 7 weeks of age. The vehicle for  
728 injections was sterile PBS + 10% Tween-80 (VWR).

#### 729 Statistical analysis

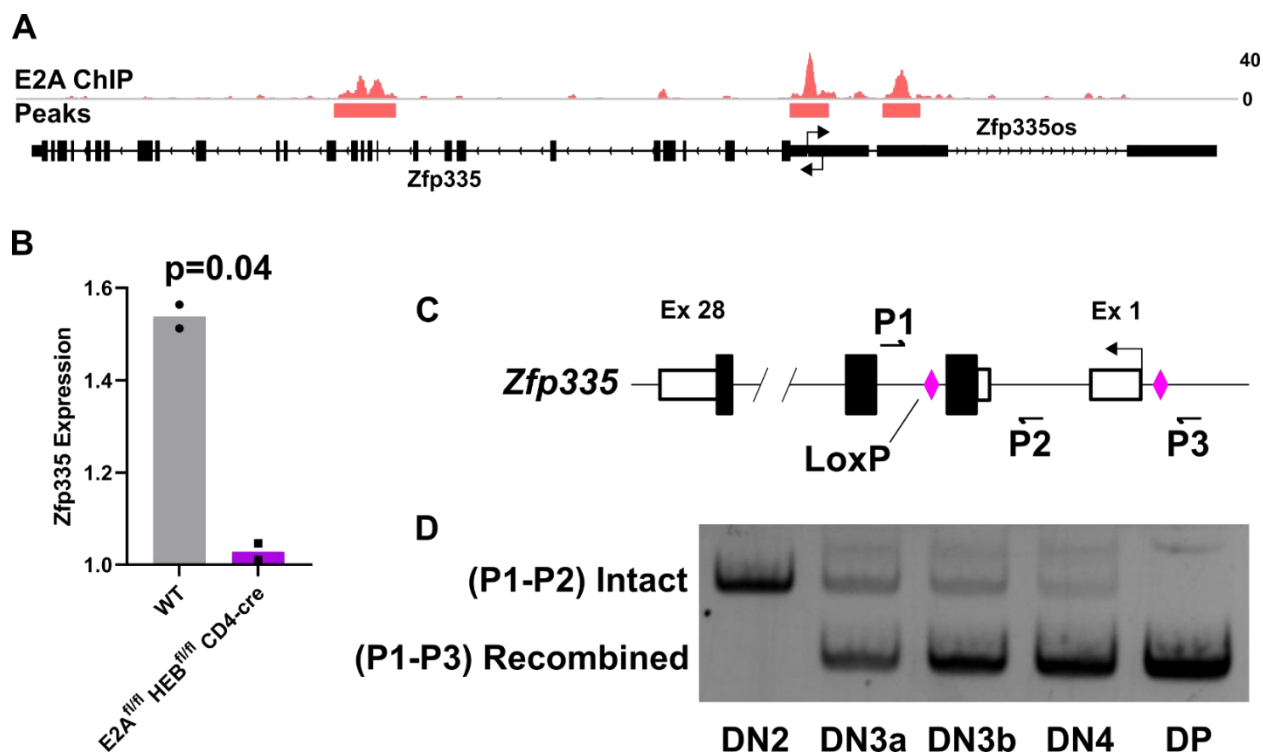
730 Statistical tests were performed using GraphPad v9.0.0 (Prism). For graphs with  
731 multiple comparisons being made, two-way ANOVA was performed with post-hoc  
732 Sidak's test or Tukey's test for multiple comparisons. For comparisons of cell numbers,  
733 data was log transformed prior to statistical tests. For all Two-way ANOVA tests  
734 normality tests were performed to ensure normalcy assumptions were met. For graphs  
735 of single comparisons, a two-tailed Mann-Whitney test was used. All significant p-values  
736 are shown in each graph. No statistical methods were used to predetermine sample  
737 size.

#### 738 **Data and code availability**

739 Data generated in this study can be accessed upon publication through NCBI Gene  
740 Expression Omnibus (<https://www.ncbi.nlm.nih.gov/geo/>) under accession GSE189244.

741

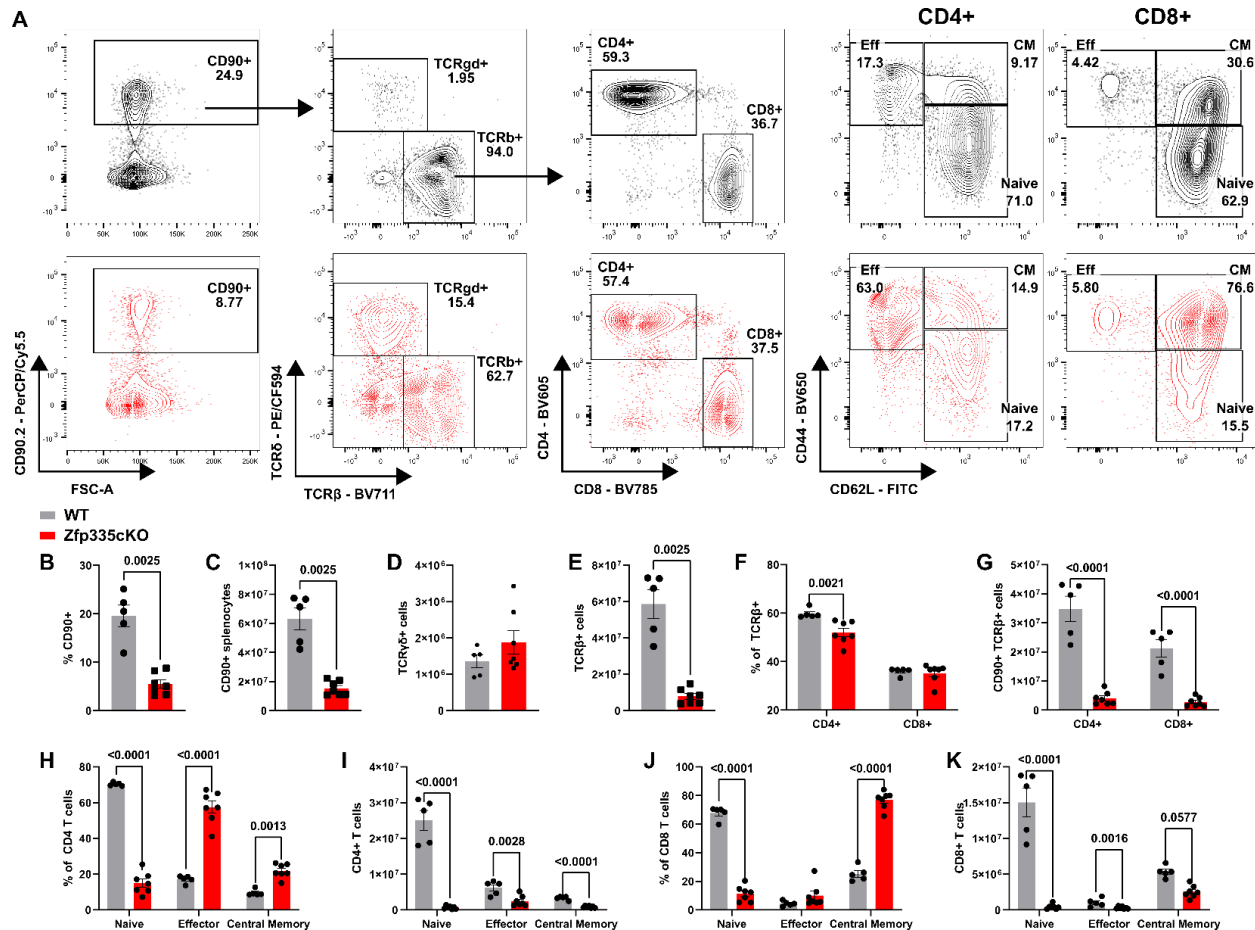
742 **Supplementary Information**



743

744 **Supplementary Figure 1 – Zfp335 is a target of E proteins in developing T cells.** (A) E2A  
745 ChIP-seq track for *Zfp335* locus in *Id2<sup>fl/fl</sup> Id3<sup>fl/fl</sup> Lck-cre* DP thymocytes (GSE89849). (B) *Zfp335*  
746 transcript abundance in WT vs. E2A/HEB double knock-out DP thymocytes determine by  
747 microarray (GSE9749). (C) Schematic diagram for PCR-based determination of *Zfp335*  
748 recombination kinetics. Small arrows indicate approximate positions for primers (P1-3)  
749 for assay. (D) Representative assessment of *Zfp335* recombination in sort purified *Zfp335<sup>fl/fl</sup> E8III-  
750 cre* DN2, DN3a, DN3b, DN4 or DP thymocytes. Data are representative of four individual  
751 experiments.

752

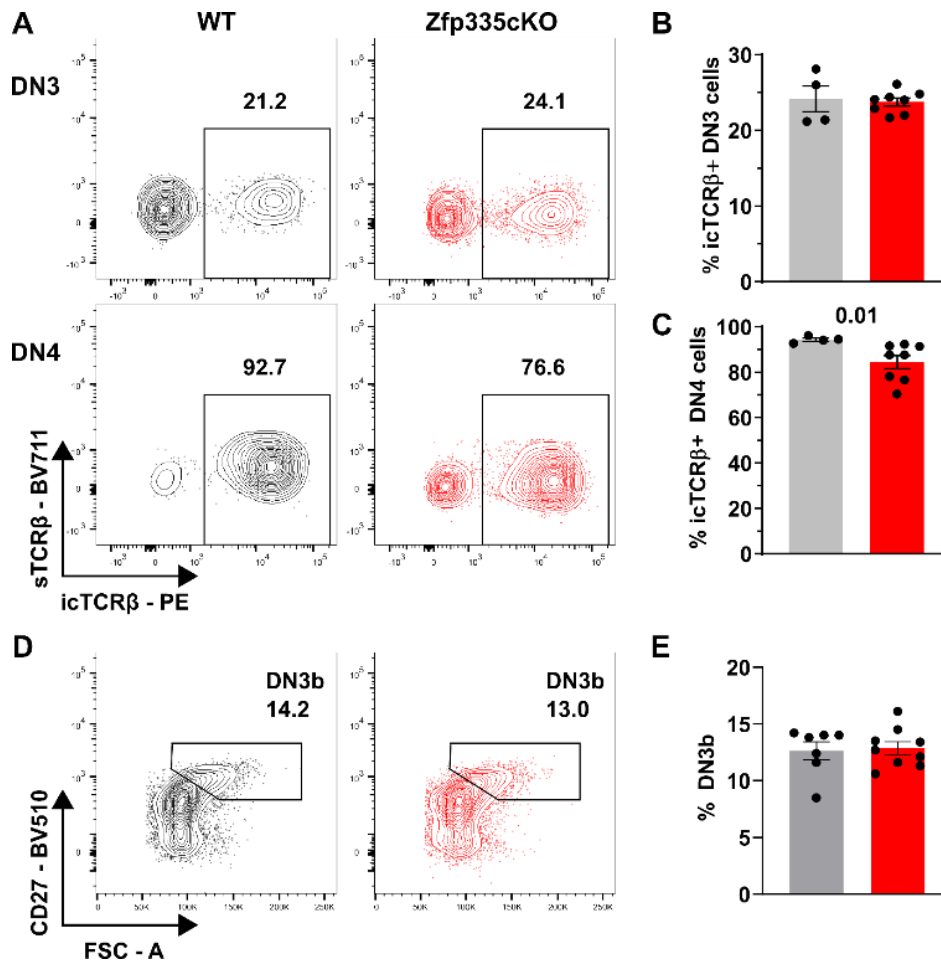


753

754 **Supplementary Figure 2 – Zfp335cKO mice exhibit T lymphopenia and reduced peripheral**  
 755 **naïve T cells.** (A) Gating schema for identification of WT (black) or Zfp335cKO (red) splenic T  
 756 cell populations beginning with live (DAPI<sup>-</sup>) splenocytes. Proportion (B) or total numbers (C) of  
 757 splenic CD90<sup>+</sup> cells. Total numbers of TCRγδ<sup>+</sup> (D) or TCRαβ<sup>+</sup> (E). Proportions (F) and total  
 758 numbers of CD4<sup>+</sup> or CD8<sup>+</sup> TCRαβ cells. Proportions (H, J) and numbers (I, K) of naïve, effector  
 759 or central memory T cells within the CD4<sup>+</sup> or CD8<sup>+</sup> compartment. WT (n=5) or Zfp335 cKO  
 760 (n=7) from two separate experiments. *P*-values determined by Mann-Whitney U-test (B-E) or  
 761 Two-Way ANOVA with *post hoc* Sidak test (F-K). Plots show mean ± sem.

762

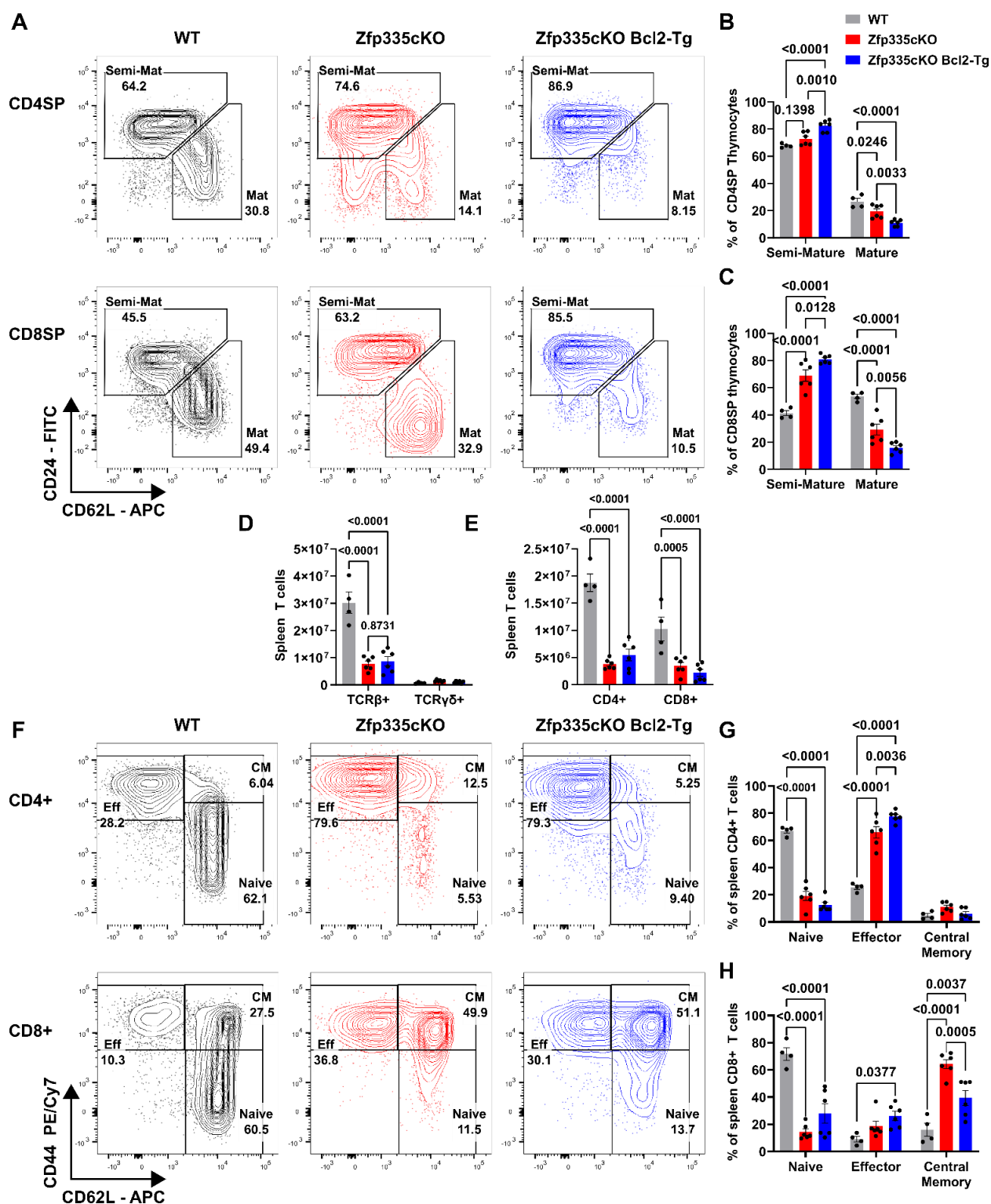




763

764 **Supplementary Figure 3 – Loss of Zfp335 during DN3 does not impair  $\beta$ -selection.** (A)  
 765 Gating for icTCR $\beta$  expression among DN3 (CD90<sup>+</sup> TCR $\delta$ <sup>-</sup> CD4<sup>-</sup> CD8<sup>-</sup> sTCR $\beta$ <sup>-</sup> CD44<sup>-</sup> CD25<sup>+</sup>) or  
 766 DN4 (CD90<sup>+</sup> TCR $\delta$ <sup>-</sup> CD4<sup>-</sup> CD8<sup>-</sup> sTCR $\beta$ <sup>-</sup> CD44<sup>-</sup> CD25<sup>-</sup>) thymocytes. Frequency of icTCR $\beta$  DN3  
 767 (B) or DN4 (C) cells among WT (n=4) or Zfp335 cKO (n=8) mice. (D) Flow cytometric gating for  
 768 identification of WT or Zfp335cKO DN3b thymocytes pre-gated on total DN3 cells. (E)  
 769 Quantification of DN3b frequency among WT or Zfp335cKO DN3 thymocytes. *P*-values  
 770 determined by Two-way ANOVA with *post hoc* Sidak test (B,C) or Mann-Whitney U-Test (E).  
 771 Plots show mean  $\pm$  sem.

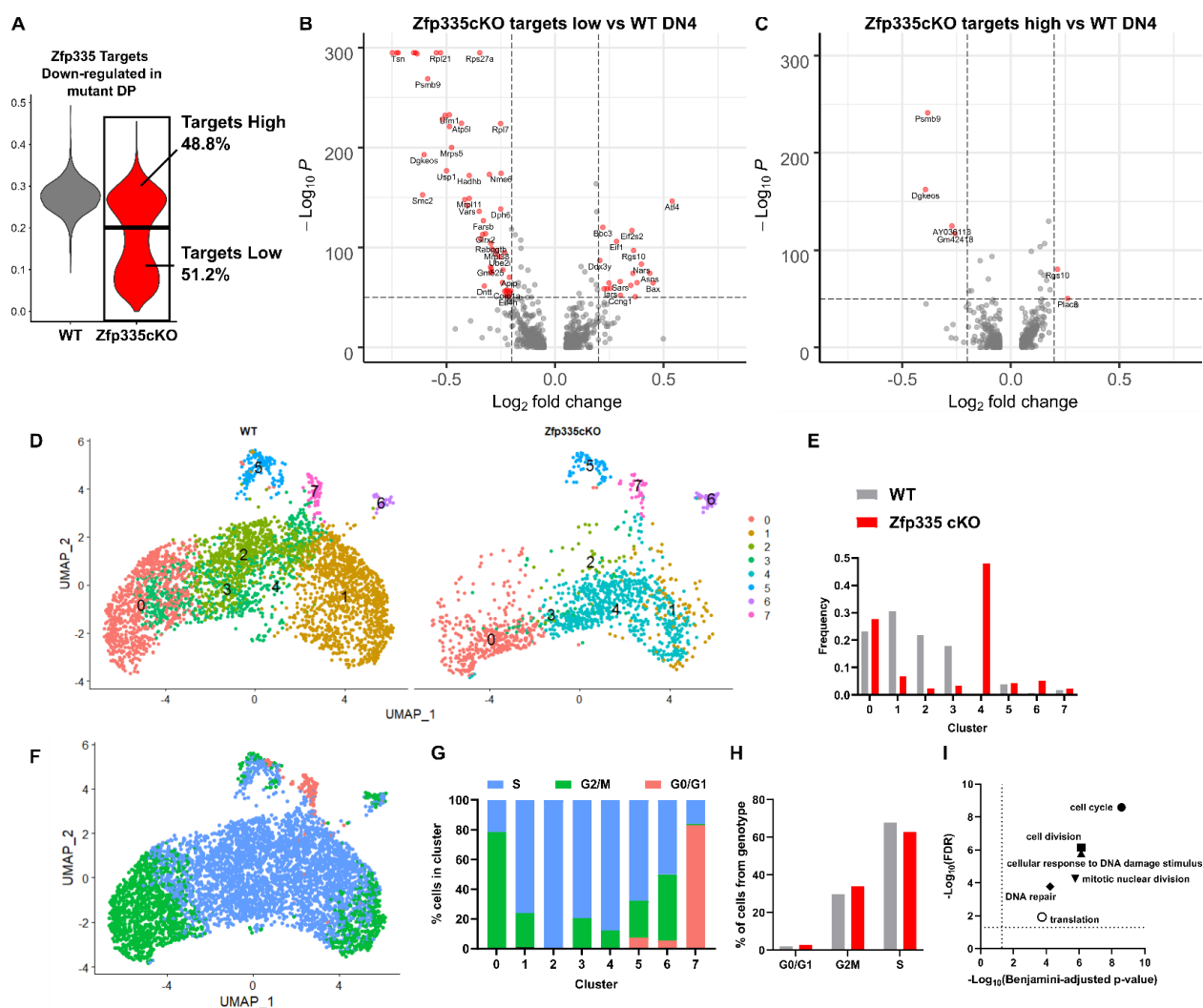
772



773  
 774 **Supplementary Figure 4 – Bcl2 overexpression fails to rescue thymic differentiation**  
 775 **defect and peripheral T lymphopenia in Zfp335-deficient mice.** Representative gating (A)  
 776 and quantification of CD4SP (B) or CD8SP (C) thymic maturation. Total splenic TCRβ and  
 777 TCRγδ (D) T cells. Quantification of total splenic CD4+ or CD8+ TCRβ+ T cells. Representative  
 778 gating (F) and quantification of splenic CD4+ (G) or CD8+ T cell effector status. n=4 WT, n=6

779 Zfp335cKO, n=6 Zfp335cKO Bcl2-Tg. Data are compiled from three independent experiments.  
 780 *P*-values determined by Two-Way ANOVA with *post hoc* Sidak Test. Plots show mean  $\pm$  sem.

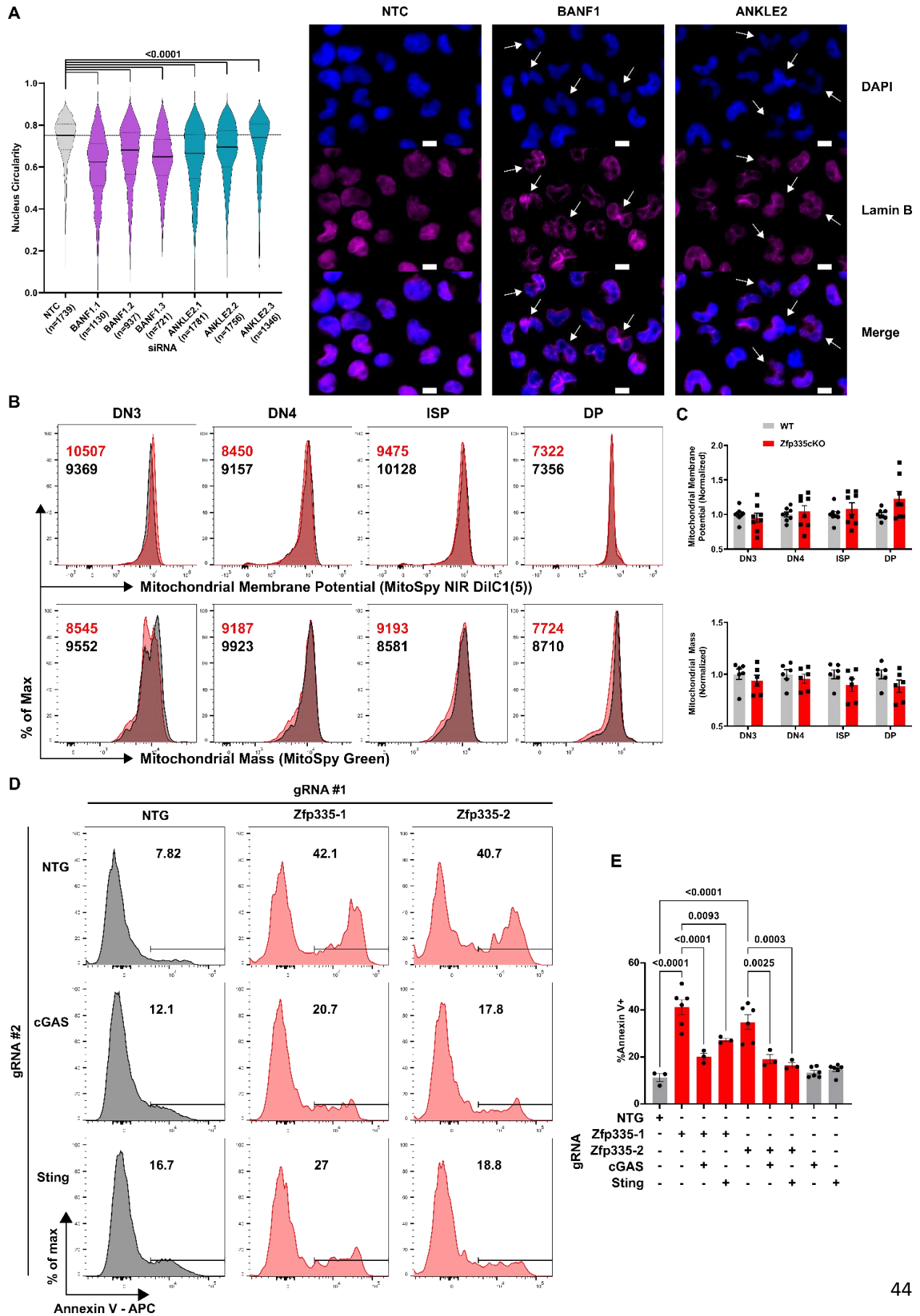
781



782

783 **Supplementary Figure 5 – scRNA-seq identifies ‘true’ Zfp335 mutant DN4 cells.** (A) Violin  
 784 plot of gene set score for Zfp335 target genes down-regulated in mutant DP thymocytes (Fig 1L-  
 785 M) and cutoff value used to identify ‘true’ Zfp335 mutant cells with low target score (lower box)  
 786 and non-mutant cells (upper box). Volcano plots of differentially expressed genes between  
 787 Zfp335cKO targets low (B) or Zfp335cKO targets high (C) cells compared with WT control. (D)  
 788 UMAP projections colored by cluster and separated by genotype for WT and true Zfp335 mutant  
 789 DN4 cells. (E) Frequency of cells found within each cluster. UMAP projection (F) and  
 790 quantification of cell cycle phase for each cluster (G). (H) Quantification of distribution of cell  
 791 cycle phase by genotype. (I) GO analysis of top 25 cluster defining genes for each cluster  
 792 (dashed lines indicate significance cutoff of  $p < 0.05$  and  $\text{FDR} < 0.05$ . *P*-values determined by  
 793 Wilcoxon Rank Sum test (B-C) or Fischer’s Exact test with Benjamini-Hochberg correction (I).

794



796 **Supplemental Figure 6 – Ankle2/BANF1 control nuclear envelope architecture.**  
 797 Quantification of nuclear circularity (A) in Hela cells transfected with non-targeting control  
 798 (NTC), BANF1-, or ANKLE2-targeting siRNAs 48 hours post-transfection (left). Representative  
 799 images DAPI or Lamin B staining of siRNA transfected Hela cells (right). Scale bars are 10µm.  
 800 Arrows indicate cells with severely disrupted nuclear envelope architecture. Representative  
 801 histograms (B) and compiled data (C) for mitochondrial membrane potential (top) or total  
 802 mitochondrial mass (bottom) in WT or Zfp335cKO thymocyte populations *ex vivo*.  
 803 Representative gating (D) and quantification (E) of Annexin V binding among DN4 cells from  
 804 *R26<sup>LSL-Cas9</sup> E8<sub>III</sub>-cre* DN3/4 thymocytes transduced with indicated gRNA-expressing retroviruses  
 805 and cultured for three days on OP9-DL1 cells. P-values calculated using One-Way ANOVA with  
 806 Dunnett's post hoc test. Plots show mean ± sem (G) or median (solid line) and interquartile  
 807 range (dotted lines) (E). Data are compiled from two (B-E) or three (F-G) independent  
 808 experiments.

809 **Table S1. Primer sequences (Related to Figures S1, 3, 5, 6 and S6)**

Primer	Gene	Sequence	Purpose
Zfp335-F	<i>Zfp335</i>	CATGTGGTTTCTGGGAAAAACT	Zfp335 <sup>fl/fl</sup> recombination
Zfp335-ex2F	<i>Zfp335</i>	GACCGTCCCAGGATTAAC	Zfp335 <sup>fl/fl</sup> recombination
Zfp335-ex2R	<i>Zfp335</i>	CTCTCCATGATCACTACCC	Zfp335 <sup>fl/fl</sup> recombination
FseI-Kz-Bcl2-F	<i>Bcl2</i>	AAGGCCGGCCGCCACCATGGCGCAAGCCGGGA	Ai6-Bcl2 cloning
Sfil-Bcl2-R	<i>Bcl2</i>	AAGGCCTGTGTGGCCTCACTTGTGGCCAGGTATGCAC	Ai6-Bcl2 cloning
Ankle2-NEB-F	<i>Ankle2</i>	AGATCTCTCGAGATCGATGCATGCTGTGGCAGCGGCTG	MSCV-Ankle2- IRES-Thy1.1 cloning
Ankle2-NEB-R	<i>Ankle2</i>	TATCGGGAATTATCGATGCATCACAGAGAAATGAAGTCCAGGGC	MSCV-Ankle2- IRES-Thy1.1 cloning
mmGapdh-F	<i>Gapdh</i>	GTCATCCCAGAGCTGAACG	RT-qPCR
mmGapdh-R	<i>Gapdh</i>	TCATACTTGGCAGGTTTCTCC	RT-qPCR
mmAnkle2-F	<i>Ankle2</i>	TTAAACCGGGACCCTTTGAT	RT-qPCR
mmAnkle2-R	<i>Ankle2</i>	ATATGAGGATGGCCCTGTGA	RT-qPCR
mmZfp335-F	<i>Zfp335</i>	CCAGGAACAGACAGTGACCAA	RT-qPCR
mmZfp335-R	<i>Zfp335</i>	CCTTCCTGGACCTGGATATGA	RT-qPCR
mmBax-F	<i>Bax</i>	TGAAGACAGGGGCCTTTTGT	RT-qPCR
mmBax-R	<i>Bax</i>	AATTCGCCGGAGACTCG	RT-qPCR
Zfp335_iT1	<i>Zfp335</i> Promoter	ttgtttGACCTCGTCGATGCCGGAGT	CRISPRi
Zfp335_iT2	<i>Zfp335</i> Promoter	ttgtttGCTGTGTGCTCTCCGACTC	CRISPRi
Zfp335_iT3	<i>Zfp335</i> Promoter	ttgtttAGGCTCAGGTTAGCGGCAGC	CRISPRi

Zfp335_iT4	<i>Zfp335</i> Promoter	ttgtttCTCAGGTTAGCGGCAGCCGG	CRISPRi
Zfp335_iT5	<i>Zfp335</i> Promoter	ttgtttCTGCCGCTAACCTGAGCCTC	CRISPRi
Zfp335_iB1	<i>Zfp335</i> Promoter	aaacACTCCGGCATCGACGAGGTCaa	CRISPRi
Zfp335_iB2	<i>Zfp335</i> Promoter	aaacGAGTCGGAGAGCGACACAGCaa	CRISPRi
Zfp335_iB3	<i>Zfp335</i> Promoter	aaacGCTGCCGCTAACCTGAGCCTaa	CRISPRi
Zfp335_iB4	<i>Zfp335</i> Promoter	aaacCCGGCTGCCGCTAACCTGAGaa	CRISPRi
Zfp335_iB5	<i>Zfp335</i> Promoter	aaacGAGGCTCAGGTTAGCGGCAGaa	CRISPRi
Zfp335_kT1	<i>Zfp335</i> exon 7	ttgtttGTACCCCGAGACCTCGACGG	<i>Ex vivo</i> CRISPR KO
Zfp335_kB1	<i>Zfp335</i> exon 7	aaacCCGTTCGAGGTCTCGGGGTACaa	<i>Ex vivo</i> CRISPR KO
Zfp335_kT2	<i>Zfp335</i> exon 16	ttgtttACCACAATCATCTACCAGCA	<i>Ex vivo</i> CRISPR KO
Zfp335_kB2	<i>Zfp335</i> exon 16	aaacTGCTGGTAGATGATTGTGGTaa	<i>Ex vivo</i> CRISPR KO
Ankle2_kT1	<i>Ankle2</i> exon 4	ttgtttGCGGAAAGCTGTGCGAAAACG	<i>Ex vivo</i> CRISPR KO
Ankle2_kB1	<i>Ankle2</i> exon 4	aaacCGTTTTTCGACAGCTTCCGCaa	<i>Ex vivo</i> CRISPR KO
Ankle2_kT2	<i>Ankle2</i> exon10	ttgtttGGGAGCTAGCTCATGAGCTG	<i>Ex vivo</i> CRISPR KO
Ankle2_kB2	<i>Ankle2</i> exon 10	aaacCAGCTCATGAGCTAGCTCCCaa	<i>Ex vivo</i> CRISPR KO
Banf1_kT1	<i>Banf1</i> exon 2	ttgtttTTGGTGACGTCTGAGCAAG	<i>Ex vivo</i> CRISPR KO
Banf1_kB1	<i>Banf1</i> exon 2	aaacCTTGCTCAGGACGTCACCAaa	<i>Ex vivo</i> CRISPR KO
Banf1_kT2	<i>Banf1</i> exon 2	ttgtttACTTCGTGGCAGAGCCCATG	<i>Ex vivo</i> CRISPR KO
Banf1_kB2	<i>Banf1</i> exon 2	aaacCATGGGCTCTGCCACGAAGTaa	<i>Ex vivo</i> CRISPR KO
Mb21d1_kT	<i>Mb21d1</i> exon 3	ttgtttTGATAAGAAGTGTACAGCA	<i>Ex vivo</i> CRISPR KO
Mb21d1_kB	<i>Mb21d1</i> exon 3	aaacTGCTGTAACACTTCTTATCAaa	<i>Ex vivo</i> CRISPR KO
Tmem173_kT	<i>Tmem173</i> exon 6	ttgtttCTACATAACAACATGCTCAG	<i>Ex vivo</i> CRISPR KO
Tmem173_kB	<i>Tmem173</i> exon 6	aaacCTGAGCATGTTGTTATGTAGaa	<i>Ex vivo</i> CRISPR KO
DsRed-NEB-F	dsRed	CCGACCTCTCTCCCAGGGGATGGATAGCACTGAGAAC	Replace



	Express II		Thy1.1 with dsRed in CRISPR KO vectors
DsRed-NEB-R	dsRed Express II	ATAAAATCTTTTATTTTATCGCTACTGGAACAGGTGGTG	Replace Thy1.1 with dsRed in CRISPR KO vectors

810

811

## 812 References

- 813 1. Krueger, A., Zietara, N. & Lyszkiewicz, M. T Cell Development by the Numbers. *Trends Immunol*  
814 **38**, 128-139 (2017).
- 815 2. Li, L., Leid, M. & Rothenberg, E.V. An early T cell lineage commitment checkpoint dependent on  
816 the transcription factor Bcl11b. *Science* **329**, 89-93 (2010).
- 817 3. Tourigny, M.R., Mazel, S., Burtrum, D.B. & Petrie, H.T. T cell receptor (TCR)-beta gene  
818 recombination: dissociation from cell cycle regulation and developmental progression during T  
819 cell ontogeny. *J Exp Med* **185**, 1549-1556 (1997).
- 820 4. Wojciechowski, J., Lai, A., Kondo, M. & Zhuang, Y. E2A and HEB are required to block thymocyte  
821 proliferation prior to pre-TCR expression. *J Immunol* **178**, 5717-5726 (2007).
- 822 5. Boudil, A. *et al.* IL-7 coordinates proliferation, differentiation and Tcr $\alpha$  recombination during  
823 thymocyte beta-selection. *Nat Immunol* **16**, 397-405 (2015).
- 824 6. Kelly, A.P. *et al.* Notch-induced T cell development requires phosphoinositide-dependent kinase  
825 1. *EMBO J* **26**, 3441-3450 (2007).
- 826 7. Guidos, C.J. Synergy between the pre-T cell receptor and Notch: cementing the alphabeta  
827 lineage choice. *J Exp Med* **203**, 2233-2237 (2006).
- 828 8. Yamasaki, S. *et al.* Mechanistic basis of pre-T cell receptor-mediated autonomous signaling  
829 critical for thymocyte development. *Nat Immunol* **7**, 67-75 (2006).
- 830 831 832 833 834 835 836

837

- 838 9. Fehling, H.J., Krotkova, A., Saint-Ruf, C. & von Boehmer, H. Crucial role of the pre-T-cell receptor  
839 alpha gene in development of alpha beta but not gamma delta T cells. *Nature* **375**, 795-798  
840 (1995).
- 841
- 842 10. Zhao, B. *et al.* Notch and the pre-TCR coordinate thymocyte proliferation by induction of the SCF  
843 subunits Fbxl1 and Fbxl12. *Nat Immunol* **20**, 1381-1392 (2019).
- 844
- 845 11. Chen, L., Foreman, D.P., Sant'Angelo, D.B. & Krangel, M.S. Yin Yang 1 Promotes Thymocyte  
846 Survival by Downregulating p53. *J Immunol* **196**, 2572-2582 (2016).
- 847
- 848 12. Bouillet, P. *et al.* BH3-only Bcl-2 family member Bim is required for apoptosis of autoreactive  
849 thymocytes. *Nature* **415**, 922-926 (2002).
- 850
- 851 13. Hutcheson, J. & Perlman, H. Loss of Bim results in abnormal accumulation of mature CD4-CD8-  
852 CD44-CD25- thymocytes. *Immunobiology* **212**, 629-636 (2007).
- 853
- 854 14. Villunger, A. *et al.* p53- and drug-induced apoptotic responses mediated by BH3-only proteins  
855 puma and noxa. *Science* **302**, 1036-1038 (2003).
- 856
- 857 15. Ren, D. *et al.* BID, BIM, and PUMA are essential for activation of the BAX- and BAK-dependent  
858 cell death program. *Science* **330**, 1390-1393 (2010).
- 859
- 860 16. Hutcheson, J. *et al.* Combined loss of proapoptotic genes Bak or Bax with Bim synergizes to  
861 cause defects in hematopoiesis and in thymocyte apoptosis. *J Exp Med* **201**, 1949-1960 (2005).
- 862
- 863 17. Rothenberg, E.V. & Taghon, T. Molecular genetics of T cell development. *Annu Rev Immunol* **23**,  
864 601-649 (2005).
- 865
- 866 18. Sawada, S. & Littman, D.R. A heterodimer of HEB and an E12-related protein interacts with the  
867 CD4 enhancer and regulates its activity in T-cell lines. *Mol Cell Biol* **13**, 5620-5628 (1993).
- 868
- 869 19. Belle, I. & Zhuang, Y. E proteins in lymphocyte development and lymphoid diseases. *Curr Top*  
870 *Dev Biol* **110**, 153-187 (2014).
- 871
- 872 20. Hsu, L.Y. *et al.* A conserved transcriptional enhancer regulates RAG gene expression in  
873 developing B cells. *Immunity* **19**, 105-117 (2003).
- 874
- 875 21. Herblot, S., Steff, A.M., Hugo, P., Aplan, P.D. & Hoang, T. SCL and LMO1 alter thymocyte  
876 differentiation: inhibition of E2A-HEB function and pre-T alpha chain expression. *Nat Immunol* **1**,  
877 138-144 (2000).



- 878  
879 22. Jia, J., Dai, M. & Zhuang, Y. E proteins are required to activate germline transcription of the TCR  
880 Vbeta8.2 gene. *Eur J Immunol* **38**, 2806-2820 (2008).
- 881  
882 23. Ghosh, J.K., Romanow, W.J. & Murre, C. Induction of a diverse T cell receptor gamma/delta  
883 repertoire by the helix-loop-helix proteins E2A and HEB in nonlymphoid cells. *J Exp Med* **193**,  
884 769-776 (2001).
- 885  
886 24. Jones, M.E. & Zhuang, Y. Stage-specific functions of E-proteins at the beta-selection and T-cell  
887 receptor checkpoints during thymocyte development. *Immunol Res* **49**, 202-215 (2011).
- 888  
889 25. Engel, I., Johns, C., Bain, G., Rivera, R.R. & Murre, C. Early thymocyte development is regulated  
890 by modulation of E2A protein activity. *J Exp Med* **194**, 733-745 (2001).
- 891  
892 26. Xu, W. *et al.* E2A transcription factors limit expression of Gata3 to facilitate T lymphocyte  
893 lineage commitment. *Blood* **121**, 1534-1542 (2013).
- 894  
895 27. Jones, M.E. & Zhuang, Y. Acquisition of a functional T cell receptor during T lymphocyte  
896 development is enforced by HEB and E2A transcription factors. *Immunity* **27**, 860-870 (2007).
- 897  
898 28. Kato, K., Omura, H., Ishitani, R. & Nureki, O. Cyclic GMP-AMP as an Endogenous Second  
899 Messenger in Innate Immune Signaling by Cytosolic DNA. *Annu Rev Biochem* **86**, 541-566 (2017).
- 900  
901 29. Sun, L., Wu, J., Du, F., Chen, X. & Chen, Z.J. Cyclic GMP-AMP synthase is a cytosolic DNA sensor  
902 that activates the type I interferon pathway. *Science* **339**, 786-791 (2013).
- 903  
904 30. Cerboni, S. *et al.* Intrinsic antiproliferative activity of the innate sensor STING in T lymphocytes. *J*  
905 *Exp Med* **214**, 1769-1785 (2017).
- 906  
907 31. Gulen, M.F. *et al.* Signalling strength determines proapoptotic functions of STING. *Nat Commun*  
908 **8**, 427 (2017).
- 909  
910 32. Li, W. *et al.* cGAS-STING-mediated DNA sensing maintains CD8(+) T cell stemness and promotes  
911 antitumor T cell therapy. *Sci Transl Med* **12** (2020).
- 912  
913 33. Wu, J., Dobbs, N., Yang, K. & Yan, N. Interferon-Independent Activities of Mammalian STING  
914 Mediate Antiviral Response and Tumor Immune Evasion. *Immunity* **53**, 115-126 e115 (2020).
- 915  
916 34. Yang, Y.J. *et al.* Microcephaly gene links trithorax and REST/NRSF to control neural stem cell  
917 proliferation and differentiation. *Cell* **151**, 1097-1112 (2012).

- 918  
919 35. Park, J.H. *et al.* Signaling by intrathymic cytokines, not T cell antigen receptors, specifies CD8  
920 lineage choice and promotes the differentiation of cytotoxic-lineage T cells. *Nat Immunol* **11**,  
921 257-264 (2010).
- 922  
923 36. Guey, B. *et al.* BAF restricts cGAS on nuclear DNA to prevent innate immune activation. *Science*  
924 **369**, 823-828 (2020).
- 925  
926 37. Engel, I. & Murre, C. The function of E- and Id proteins in lymphocyte development. *Nat Rev*  
927 *Immunol* **1**, 193-199 (2001).
- 928  
929 38. Engel, I. & Murre, C. E2A proteins enforce a proliferation checkpoint in developing thymocytes.  
930 *EMBO J* **23**, 202-211 (2004).
- 931  
932 39. Jones-Mason, M.E. *et al.* E protein transcription factors are required for the development of  
933 CD4(+) lineage T cells. *Immunity* **36**, 348-361 (2012).
- 934  
935 40. Roy, S. *et al.* Id Proteins Suppress E2A-Driven Invariant Natural Killer T Cell Development prior to  
936 TCR Selection. *Front Immunol* **9**, 42 (2018).
- 937  
938 41. Dashtsoodol, N. *et al.* Alternative pathway for the development of Valpha14(+) NKT cells directly  
939 from CD4(-)CD8(-) thymocytes that bypasses the CD4(+)CD8(+) stage. *Nat Immunol* **18**, 274-282  
940 (2017).
- 941  
942 42. Han, B.Y. *et al.* Zinc finger protein Zfp335 is required for the formation of the naive T cell  
943 compartment. *Elife* **3** (2014).
- 944  
945 43. Haks, M.C., Krimpenfort, P., van den Brakel, J.H. & Kruisbeek, A.M. Pre-TCR signaling and  
946 inactivation of p53 induces crucial cell survival pathways in pre-T cells. *Immunity* **11**, 91-101  
947 (1999).
- 948  
949 44. Taghon, T., Yui, M.A., Pant, R., Diamond, R.A. & Rothenberg, E.V. Developmental and molecular  
950 characterization of emerging beta- and gammadelta-selected pre-T cells in the adult mouse  
951 thymus. *Immunity* **24**, 53-64 (2006).
- 952  
953 45. Holmes, R. & Zuniga-Pflucker, J.C. The OP9-DL1 system: generation of T-lymphocytes from  
954 embryonic or hematopoietic stem cells in vitro. *Cold Spring Harb Protoc* **2009**, pdb prot5156  
955 (2009).
- 956  
957 46. Mingueneau, M. *et al.* The transcriptional landscape of alphabeta T cell differentiation. *Nat*  
958 *Immunol* **14**, 619-632 (2013).

- 959  
960 47. Miller, D.G., Adam, M.A. & Miller, A.D. Gene transfer by retrovirus vectors occurs only in cells  
961 that are actively replicating at the time of infection. *Mol Cell Biol* **10**, 4239-4242 (1990).
- 962  
963 48. Trang, N.V. *et al.* Determination of cut-off cycle threshold values in routine RT-PCR assays to  
964 assist differential diagnosis of norovirus in children hospitalized for acute gastroenteritis.  
965 *Epidemiol Infect* **143**, 3292-3299 (2015).
- 966  
967 49. Asencio, C. *et al.* Coordination of kinase and phosphatase activities by Lem4 enables nuclear  
968 envelope reassembly during mitosis. *Cell* **150**, 122-135 (2012).
- 969  
970 50. Carleton, M. *et al.* Signals transduced by CD3epsilon, but not by surface pre-TCR complexes, are  
971 able to induce maturation of an early thymic lymphoma in vitro. *J Immunol* **163**, 2576-2585  
972 (1999).
- 973  
974 51. Tanenbaum, M.E., Gilbert, L.A., Qi, L.S., Weissman, J.S. & Vale, R.D. A protein-tagging system for  
975 signal amplification in gene expression and fluorescence imaging. *Cell* **159**, 635-646 (2014).
- 976  
977 52. Ma, H. *et al.* Barrier-to-Autointegration Factor 1 Protects against a Basal cGAS-STING Response.  
978 *mBio* **11** (2020).
- 979  
980 53. Larkin, B. *et al.* Cutting Edge: Activation of STING in T Cells Induces Type I IFN Responses and Cell  
981 Death. *J Immunol* **199**, 397-402 (2017).
- 982  
983 54. Zierhut, C. & Funabiki, H. Regulation and Consequences of cGAS Activation by Self-DNA. *Trends*  
984 *Cell Biol* **30**, 594-605 (2020).
- 985  
986 55. McArthur, K. *et al.* BAK/BAX macropores facilitate mitochondrial herniation and mtDNA efflux  
987 during apoptosis. *Science* **359** (2018).
- 988  
989 56. Vincent, J. *et al.* Small molecule inhibition of cGAS reduces interferon expression in primary  
990 macrophages from autoimmune mice. *Nat Commun* **8**, 750 (2017).
- 991  
992 57. Haag, S.M. *et al.* Targeting STING with covalent small-molecule inhibitors. *Nature* **559**, 269-273  
993 (2018).
- 994  
995 58. Zhang, B. *et al.* Differential Requirements of TCR Signaling in Homeostatic Maintenance and  
996 Function of Dendritic Epidermal T Cells. *J Immunol* **195**, 4282-4291 (2015).
- 997  
998 59. Lucas, B. & Germain, R.N. Unexpectedly complex regulation of CD4/CD8 coreceptor expression  
999 supports a revised model for CD4+CD8+ thymocyte differentiation. *Immunity* **5**, 461-477 (1996).

- 1000  
1001 60. Agata, Y. *et al.* Regulation of T cell receptor beta gene rearrangements and allelic exclusion by  
1002 the helix-loop-helix protein, E47. *Immunity* **27**, 871-884 (2007).
- 1003  
1004 61. Petersson, K., Ivars, F. & Sigvardsson, M. The pT alpha promoter and enhancer are direct targets  
1005 for transactivation by E box-binding proteins. *Eur J Immunol* **32**, 911-920 (2002).
- 1006  
1007 62. Wang, D. *et al.* The basic helix-loop-helix transcription factor HEBAIt is expressed in pro-T cells  
1008 and enhances the generation of T cell precursors. *J Immunol* **177**, 109-119 (2006).
- 1009  
1010 63. Link, N. *et al.* Mutations in ANKLE2, a ZIKA Virus Target, Disrupt an Asymmetric Cell Division  
1011 Pathway in Drosophila Neuroblasts to Cause Microcephaly. *Dev Cell* **51**, 713-729 e716 (2019).
- 1012  
1013 64. Yamamoto, S. *et al.* A drosophila genetic resource of mutants to study mechanisms underlying  
1014 human genetic diseases. *Cell* **159**, 200-214 (2014).
- 1015  
1016 65. Matsui, T.K. & Mori, E. Microglia support neural stem cell maintenance and growth. *Biochem*  
1017 *Biophys Res Commun* **503**, 1880-1884 (2018).
- 1018  
1019 66. Shigemoto-Mogami, Y., Hoshikawa, K., Goldman, J.E., Sekino, Y. & Sato, K. Microglia enhance  
1020 neurogenesis and oligodendrogenesis in the early postnatal subventricular zone. *J Neurosci* **34**,  
1021 2231-2243 (2014).
- 1022  
1023 67. Ribeiro Xavier, A.L., Kress, B.T., Goldman, S.A., Lacerda de Menezes, J.R. & Nedergaard, M. A  
1024 Distinct Population of Microglia Supports Adult Neurogenesis in the Subventricular Zone. *J*  
1025 *Neurosci* **35**, 11848-11861 (2015).
- 1026  
1027 68. Reinert, L.S. *et al.* Brain immune cells undergo cGAS/STING-dependent apoptosis during herpes  
1028 simplex virus type 1 infection to limit type I IFN production. *J Clin Invest* **131** (2021).
- 1029  
1030 69. Yang, K. *et al.* Metabolic signaling directs the reciprocal lineage decisions of alphabeta and  
1031 gammadelta T cells. *Sci Immunol* **3** (2018).
- 1032  
1033 70. Sanson, K.R. *et al.* Optimized libraries for CRISPR-Cas9 genetic screens with multiple modalities.  
1034 *Nat Commun* **9**, 5416 (2018).
- 1035  
1036